



RESEARCH ARTICLE

Blue light induces apoptosis and autophagy by promoting ROS-mediated mitochondrial dysfunction in synovial sarcoma

Makoto Takeuchi¹  | Toshihiko Nishisho¹ | Shunichi Toki¹  | Shinji Kawaguchi¹ | Shunsuke Tamaki¹ | Takeshi Oya² | Yoshihiro Uto³ | Toyomasa Katagiri⁴ | Koichi Sairyo¹

¹Department of Orthopedics, Institute of Biomedical Sciences, Tokushima University Graduate School, Tokushima, Japan

²Department of Molecular Pathology, Institute of Biomedical Sciences, Tokushima University Graduate School, Tokushima, Japan

³Graduate School of Technology, Industrial and Social Sciences, Tokushima University, Tokushima, Japan

⁴Division of Genome Medicine, Institute of Advanced Medical Sciences, Tokushima University, Tokushima, Japan

Correspondence

Toshihiko Nishisho, Department of Orthopedics, Institute of Biomedical Sciences, Tokushima University Graduate School, 3-18-15 Kuramotocho, Tokushima, Tokushima, 770-8503, Japan.

Email: tnishisho@gmail.com

Abstract

Background: Synovial sarcoma (SS) has limited treatment options and there is an urgent need to develop a novel therapeutic strategy to treat SS. Blue light (BL) has been shown to inhibit the growth of several cancer cells. However, the efficacy of BL in soft tissue sarcomas such as SS has not been demonstrated, and the detailed mechanism underlying the antitumor activity of BL is not fully understood. In this study, we investigated the antitumor effect of BL on SS.

Methods: Human SS cell lines were continuously irradiated with BL using light-emitting diodes (LEDs) in an incubator for in vitro analysis. The chicken chorio-allantoic membrane (CAM) tumors and xenograft tumors in mice were subjected to daily BL irradiation with LEDs.

Results: BL caused growth inhibition of SS cells and histological changes in CAM tumors. BL also suppressed the migration and invasion abilities of SS cells. The type of cell death in SS cells was revealed to be apoptosis. Furthermore, BL induced excessive production of reactive oxygen species (ROS) in mitochondria, resulting in oxidative stress and malfunctioned mitochondria. Reducing the production of ROS using N-acetylcysteine (NAC), a ROS scavenger, attenuated the inhibitory effect of BL on SS cells and mitochondrial dysfunction. In addition, BL induced autophagy, which was suppressed by the administration of NAC. The autophagy inhibitor of 3-methyladenine and small interfering RNA against the autophagy marker light chain 3B facilitated apoptotic cell death. Moreover, BL suppressed tumor growth in a mouse xenograft model.

Conclusion: Taken together, our results revealed that BL induced apoptosis via the ROS-mitochondrial signaling pathway, and autophagy was activated in response to the production of ROS, which protected SS cells from apoptosis. Therefore, BL is a promising candidate for the development of an antitumor therapeutic strategy targeting SS.

This is an open access article under the terms of the [Creative Commons Attribution](https://creativecommons.org/licenses/by/4.0/) License, which permits use, distribution and reproduction in any medium, provided the original work is properly cited.

© 2023 The Authors. *Cancer Medicine* published by John Wiley & Sons Ltd.

KEYWORDS

apoptosis, autophagy, blue light, mitochondria, reactive oxygen species, synovial sarcoma

1 | INTRODUCTION

Synovial sarcoma (SS) is a highly malignant soft tissue tumor that can arise in various parts of the body, but most that tend to arise from sites near joints, including the bursae, joint capsules, and tendon sheaths. Accounting for 5%–10% of all soft tissue sarcomas, SS is the fourth most frequent soft tissue tumor.¹ The current treatment for localized SS is surgical excision with a broad margin of the surrounding normal tissue, occasionally with combined radiotherapy and chemotherapy. The 5-year survival rate is estimated to be 40%–60%,^{2,3} but when lung metastases develop or there is recurrence of the primary tumor, the prognosis is poor, even with intensive multidrug chemotherapy. Because of the limited availability of effective treatments, there is an urgent need to develop novel therapies for patients with SS.

In the present era, humans can conveniently control visible light in a specific narrow wavelength owing to the invention and development of light-emitting diodes (LEDs), which are a novel luminous source dating back to the late 1900s. In medicine, phototherapy using LEDs is widely used for several therapeutic targets including acne vulgaris,⁴ wound healing,⁵ skin rejuvenation,⁶ and bacterial and viral infections.^{7,8} Furthermore, light irradiation at wavelengths ranging from 450 to 495 nm, which human eyes perceive as blue, has been shown to have antitumor effects on various cancer cells, including melanoma,^{9,10} lymphoma,¹¹ colon cancer,^{12–15} leukemia,¹⁶ pancreatic cancer,¹⁷ and osteosarcoma.¹⁸ Therefore, blue light (BL) from LEDs is expected to become a novel non-invasive therapeutic option in cancer treatment. Although the biological mechanism of BL-induced antitumor effect is reported to be regulated by cell cycle inhibition,⁹ reactive oxygen species,^{18–21} apoptosis,^{9,12,17,20,22} and autophagy,^{11,12,14,18} its role and precise mechanisms remain unclear. Despite the beneficial effects of BL on various cancers, to date, the efficacy and biological response to BL in soft tissue sarcoma including SS has yet to be determined.

In this study, we investigated the ability of BL to inhibit growth in SS cells *in vitro* and *in vivo* and elucidated the underlying mechanisms. Our findings provide direct evidence that BL might exert antitumor effects on SS and may therefore be a novel treatment option for SS.

2 | MATERIALS AND METHODS

2.1 | Cell culture

The human SS cell lines SYO-1, HS-SY-II, Aska-SS, and Yamato-SS as well as the human embryonic kidney cell line HEK293 were used. SYO-1 was donated by Dr. Akira Kawai (National Cancer Center Hospital),²³ while HS-SY-II, Aska-SS, Yamato-SS, and HEK293 were purchased from the RIKEN BioResource Center Cell Bank. SS cells from surgical specimens were isolated using collagenase (Sigma-Aldrich) according to a previously published protocol.²⁴ Informed consent was obtained from the patients according to institutional guidelines. The clinicopathological data of the SS patients are shown in Table S1. All cells were cultured in Dulbecco's modified Eagle medium (Sigma-Aldrich) supplemented with 10% fetal bovine serum (FBS; Sigma-Aldrich) and penicillin/streptomycin (Sigma-Aldrich) in a humidified atmosphere of 5% CO₂ at 37°C. The chemical reagents used in this study are listed in Table S2.

2.2 | Light irradiation

For the *in vitro* experiments, Teleopto LED array systems (LEDA-X LED Array with LAD-1 driver; Amuza) were used. The cells received continuous light irradiation in a CO₂ incubator with blue (peak at 470 nm), green (peak at 525 nm), or red (peak at 630 nm) light. For *in vivo* experiments or the chorioallantoic membrane (CAM) assay, LED chips (WS2812B; WorldSemi) were used at a light intensity of 30 mW/cm², which peak at 470 nm for the output of BL. The light intensity was measured with a Light Power Meter (LPM-100; Amuza). After BL irradiation, the samples were used for further study. See the Data S1 for further details on the experimental methods.

2.3 | CAM assay

Fertilized chicken eggs were purchased from the Goto farm in Gifu, Japan. The fertilized chicken eggs were kept in a humidified egg incubator at 37°C. After 11 days of incubation, a window on the eggshell was made. For transplantation, a sterile Teflon ring (Sansyo) was placed at the Y-shape blood vessel on the CAM. Then, 20 μL of a cellular suspension containing 5 × 10⁵ SYO-1 cells in

growth medium were grafted into the ring and the window was covered with clear film. And 4 days after transplantation, irradiation with BL (30 mW/cm²) was started continuously. One week after transplantation, CAM tumors were resected and fixed in 4% paraformaldehyde. Hematoxylin and eosin (H&E) staining and TUNEL analysis were conducted as described in Data S1.

2.4 | In vivo xenograft tumor model

Male BALB/c nude mice were purchased from SLC Japan at 4 weeks of age. All animal experiments were performed in accordance with the university's guidelines on the ethical care and use of animals. The mice were kept in the laboratory for 1 week to adapt to the rearing environment. Then 100 μ L cellular suspension containing 5×10^6 SYO-1 cells in PBS were injected subcutaneously into the left flank of the mice. One week after injection, the mice were randomly divided into two groups: control group (CTL, $n = 8$) and BL group (BL, $n = 8$). Mice in the BL group were fixed on cages using adhesive tapes and irradiated with BL (30 mW/cm²) for 8 h/day for 12 days. Mice in the CTL group were fixed in the same manner without BL irradiation. Body weight was measured every 2 or 3 days, the long and short diameters of the tumor were measured using an electronic caliper, and the tumor volume was calculated. After BL irradiation, the mice were sacrificed. The tumors were extracted, weighed, and used for further study.

2.5 | Statistical analyses

Plot and statistical tests were generated with GraphPad Prism 9 (GraphPad Software). Data are presented as the mean \pm standard error of the mean. All results were confirmed in at least three independent experiments. An unpaired Student's *t*-test or one-way analysis of variance was used to calculate the significance between different groups. $p < 0.05$ was considered statistically significant.

3 | RESULTS

3.1 | BL inhibits viability and colony formation of SS cells and induces histological changes in the CAM SS tumor model

The cells received light irradiation continuously in a CO₂ incubator and were subjected to biological analyses (Figure 1A). The CCK-8 assay showed that BL inhibited the viability of SYO-1, HS-SY-II, Saka-SS, and Yamato-SS cells in both a light intensity- and time-dependent manner (Figure 1B). In addition, the colony formation ability

of SS cells was markedly suppressed by BL (0.1 mW/cm²) for 24 h (Figure 1C,D). To determine whether the effect of light irradiation on SS cells varied depending on the wavelength, SS cells were separately irradiated with three different wavelengths of light, blue (peak at 470 nm), green (peak at 525 nm), or red (peak at 630 nm) at a unified intensity of 0.6 mW/cm² for 48 h. As a result, only the inhibition of BL for each cell line was exhibited (Figure S1A). To determine whether BL also has effects on primary human SS cells, primary SS cells isolated from two SS patients (P1 and P2) were irradiated with BL (0.6 mW/cm²). As shown in Figure 1E, BL irradiation resulted in the decreased viability of primary SS cells in a time-dependent manner. The growth-inhibitory effect of BL on HEK293, a non-cancer cell line, was also examined, and a growth-inhibitory effect was observed that was similar to the results for the SS cell lines (Figure S1B).

Next, to verify whether BL has antitumor effects on three-dimensional structural tissues as tumors in addition to two-dimensional planar structures such as cultured cells, we performed a CAM assay as a preliminary step before in vivo experiments (Figure 1F). H&E staining of CAM SS tumor tissues irradiated with BL showed decreased cellularity and vacuolar changes in the cytoplasm of tumor cells compared to CTL (Figure 1G), and TUNEL analysis showed a significant increase in the number of TUNEL-positive cells (Figure 1G,H).

3.2 | BL suppresses the migration and invasion of SS cells

To investigate the molecular mechanism underlying the growth-inhibitory effect of BL on SS cells, we performed microarray analysis in which SYO-1 cells were incubated with or without BL (0.6 mW/cm²) for 48 h. The volcano plot of the differentially expressed genes (DEGs) indicated that there were 1131 DEGs in BL-irradiated SS cells compared with CTL ones, among which 605 DEGs were significantly upregulated and 526 were significantly downregulated. Differences in expression levels were defined by cutoff \log_2 (fold change) > 1 and corrected $p > 0.05$ (Figure S2A). Unsupervised hierarchical clustering analysis of these genes revealed a clear separation of DEGs between BL-irradiated cells and CTL cells (Figure S2B). To further characterize the overarching biological process, gene set enrichment analysis (GSEA) of the hallmark and Gene Ontology gene sets were performed. Table S3 shows the top upregulated or downregulated gene sets based on a normalized enrichment score (NES) of > 1.5 or < -1.5 and a normal p -value of < 0.05 as the threshold.

The results of GSEA showed a negative correlation for metastasis_up and a positive correlation for metastasis_down, indicating that BL inhibits metastasis of SS cells (Figure 2A). To verify the inhibitory effect of BL on the

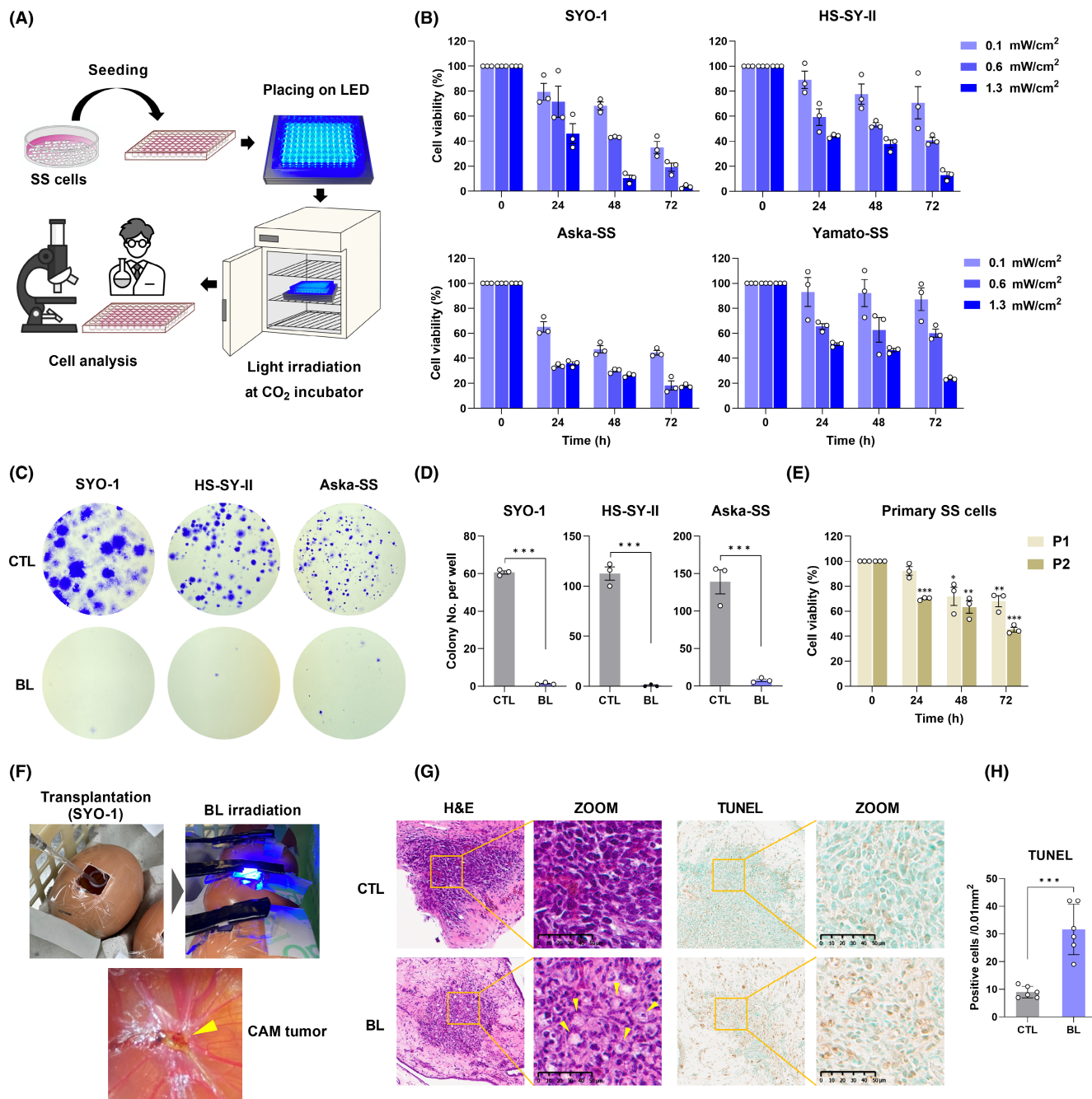
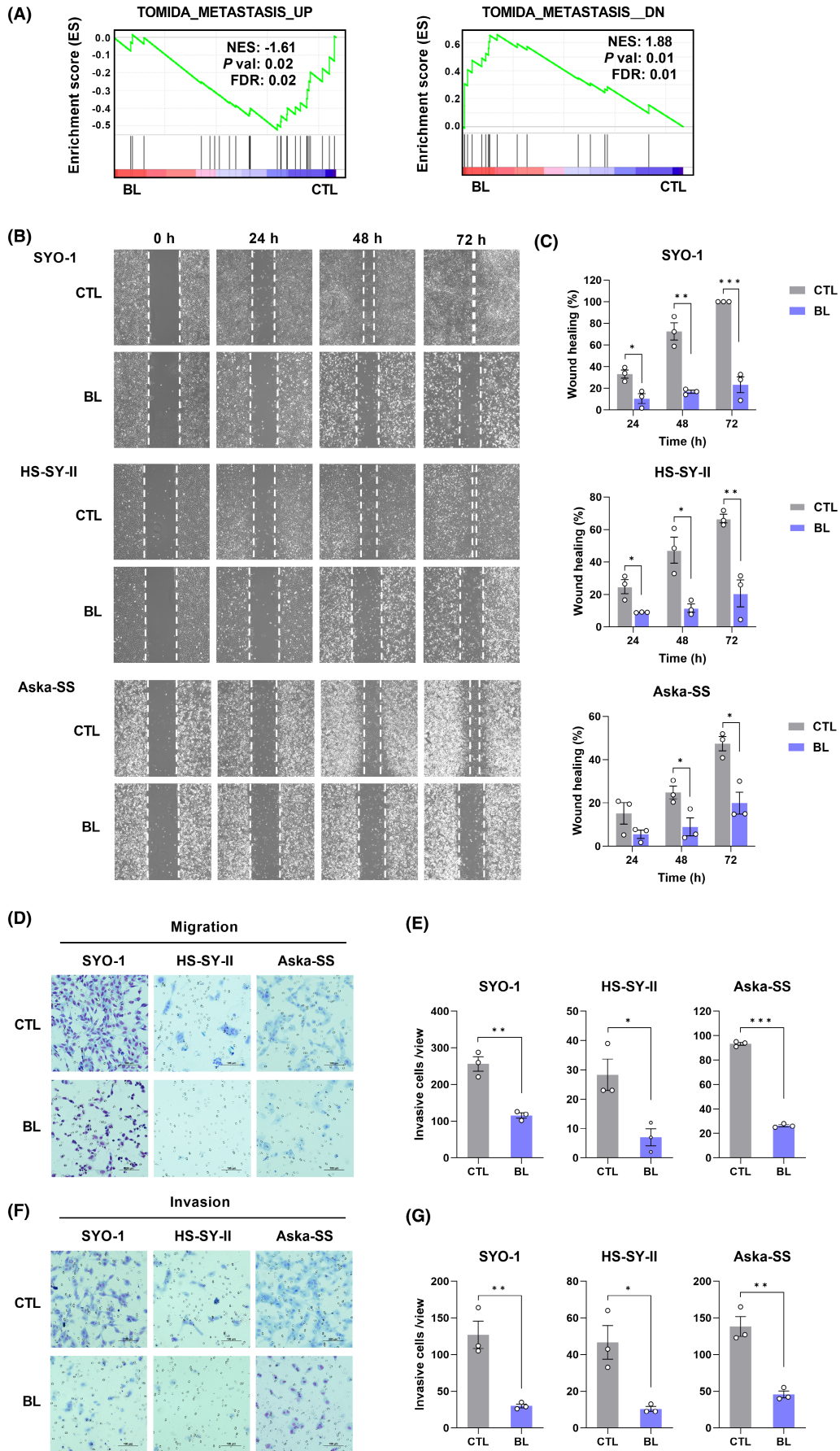


FIGURE 1 Blue light (BL) inhibited the proliferation and colony formation capacity of synovial sarcoma (SS) cells and induced a histological change in chorioallantoic membrane (CAM) tumor tissues. (A) Schematic illustration of the experimental protocol using LED devices in vitro. (B) A CCK-8 assay was used to measure cell viability. (C) Colony formation assay of SS cells incubated with or without BL irradiation (0.1 mW/cm²) for 24h. (D) Quantification of the mean number of colonies formed in each group. (E) A CCK-8 assay was used to measure the cell viability of primary SS cells from two patients with SS (P1 and P2). (F) Images of BL irradiation in the CAM assay. The yellow arrow indicates the formation of a tumor-like structure. (G) H&E staining was used to evaluate the histology. The yellow arrows indicate vacuolar change in the cytoplasm of tumor cells. The apoptotic status of tumor tissues was assessed by the TUNEL assay. (H) Quantification of TUNEL-positive cells per field. Data are presented as the mean ± standard error of the mean (SEM) of three independent experiments. ****p* < 0.001.

FIGURE 2 Blue light (BL) suppressed the migration and invasion abilities of synovial sarcoma (SS) cells. (A) gene set enrichment analysis (GSEA) of microarray data. NES, normalized enrichment score; FDR, false discovery rate. (B) Wound healing assay of SS cells. (C) Quantification of the mean percentage of wound healing in each group. (D) The migration abilities were analyzed using Transwell filters. (E) Quantification of the mean number of migrated cells in each group. (F) Invasion ability was analyzed using Matrigel-coated Transwell filters. (G) Quantification of the mean number of invasive cells in each group. Data are presented as the mean ± SEM of three independent experiments. **p* < 0.05, ***p* < 0.01, ****p* < 0.001.



migration ability of SS cells, we performed a wound healing assay, which showed that BL (0.6 mW/cm²) reduced the migration ability of SYO-1, HS-SY-II, and Aska-SS cells (Figure 2B,C). Furthermore, we performed Transwell experiments and found that the migration and invasion abilities of SS cells were much lower in BL-irradiated cells compared with CTL cells (Figure 2D–G).

3.3 | BL induces apoptosis in SS cells

Among related gene sets in GSEA, apoptosis-related signatures were enriched (Figure 3A); therefore, we first investigated whether BL promoted apoptosis in SS cells. Annexin V-FITC/PI double staining with flow cytometry showed that BL (0.6 mW/cm²) significantly increased the proportion of apoptotic SYO-1 and HS-SY-II cells in a time-dependent manner (Figure 3B,C). Next, cell cycle analysis was performed to determine whether inhibition of cell proliferation was caused by cell cycle arrest. To clarify the protein underlying BL-induced apoptosis, we showed that BL (0.6 mW/cm²) markedly induced the expression of cleaved PARP in SYO-1 and HS-SY-II cells (Figure 3D). To determine whether caspase activation was directly involved in BL-induced apoptotic events, CellEvent fluorogenic substrate was utilized via flow cytometry. Caspase 3/7 activation was detectable in BL (0.6 mW/cm²)-irradiated SYO-1 and HS-SY-II cells in a time-dependent manner (Figure 3E). Additionally, to better characterize whether BL-induced cell death was caspase-dependent, the cells were irradiated with BL in the presence or absence of the pan-caspase inhibitor, Z-VAD-FMK (Z-VAD). BL (0.6 mW/cm²) with Z-VAD (100 μM) for 48 h sufficiently rescued cell viability (Figure 3F) and decreased the number of apoptotic cells, according to an Annexin V-FITC/PI assay of SYO-1 and HS-SY-II cells (Figure 3G,H). These findings suggest that BL induces apoptosis by caspase activation in SS cells.

3.4 | ROS are critical for the BL-induced apoptosis of SS cells

GSEA of microarray data showed that ROS-related signatures were enriched (Figure 4A). To verify ROS production in BL-irradiated SYO-1 cells, the CellROX probe was initially used. As shown in Figure S3A,B, irradiation with BL (0.6 mW/cm²) for 48 h increased the percentage of cells with green fluorescence. The major source of ROS in cells is mitochondria²⁵; therefore, we next investigated whether ROS formation linked to BL irradiation occurred in the mitochondria. We used MitoSOX, a probe that specifically detects ROS produced in mitochondria. As expected, BL

irradiation caused enhanced ROS production in the mitochondria (Figure 4B,C).

GSEA analysis of microarray data also showed gene enrichment in the cellular oxidant detoxification and anti-oxidant activity in BL-irradiated SYO-1 cells (Figure S3C). Overproduction of ROS caused by BL was expected to result in oxidative stress as well as induce cytoprotective and antioxidant activity in SS cells. In the analysis of gene expression of HO-1,²⁶ oxidative stress-induced growth inhibitor 1 (OSGIN1),²⁷ and NAD(P)H:quinone oxidoreductase 1 (NQO1),²⁸ which are related to oxidative stress, the mRNA levels of BL-irradiated SS cells were higher than those of CTL cells (Figure S3D). Western blot analysis showed that SYO-1 and HS-SY-II cells irradiated with BL (0.6 mW/cm²) sharply increased protein expression of HO-1 (Figure 4D), which is a rate-limiting enzyme in heme catabolism and plays a key role in inducible antioxidant defenses.^{29,30} These results revealed that BL increased the production of mitochondrial ROS, causing oxidative stress in SS cells.

In addition, considering that overaccumulation of ROS might cause the apoptotic death of SS cells, the experiments were performed using BL irradiation with or without N-acetyl-cysteine (NAC), a ROS scavenger. NAC (5 mM) significantly reversed the inhibition of cell viability induced by BL (0.6 mW/cm²) for 48 h (Figure 4E) and decreased the number of apoptotic cells in the Annexin V-FITC/PI assay (Figure 4F,G). The protein expression of HO-1 and cleaved PARP was downregulated in SYO-1 and HS-SY-II cells irradiated with BL (0.6 mW/cm²) combined with NAC (5 mM) for 48 h compared with cells irradiated with BL alone (Figure 4H). These results demonstrated that mitochondrial ROS mediates BL-induced apoptosis in SS cell lines.

3.5 | BL triggers the mitochondrial dysfunction caused by ROS production

GSEA of microarray data indicated the positive regulation of cytochrome c release from mitochondria in BL-irradiated cells (Figure 5A). Some sort of stress signal may trigger mitochondrial dysfunction, resulting in the release of cytochrome c and thereby causing caspase activation and apoptosis.³¹ Next, we investigated whether BL might amplify mitochondrial dysfunction in SS cells. Because the mitochondrial oxidative phosphorylation process may be affected by mitochondrial dysfunction, we first investigated the mitochondrial respiratory capacity, using the Seahorse XF HS analyzer. The OCR, an indicator of mitochondrial respiration, showed that BL (0.6 mW/cm²) for 48 h remarkably suppressed basal respiration, ATP production, maximal respiration,

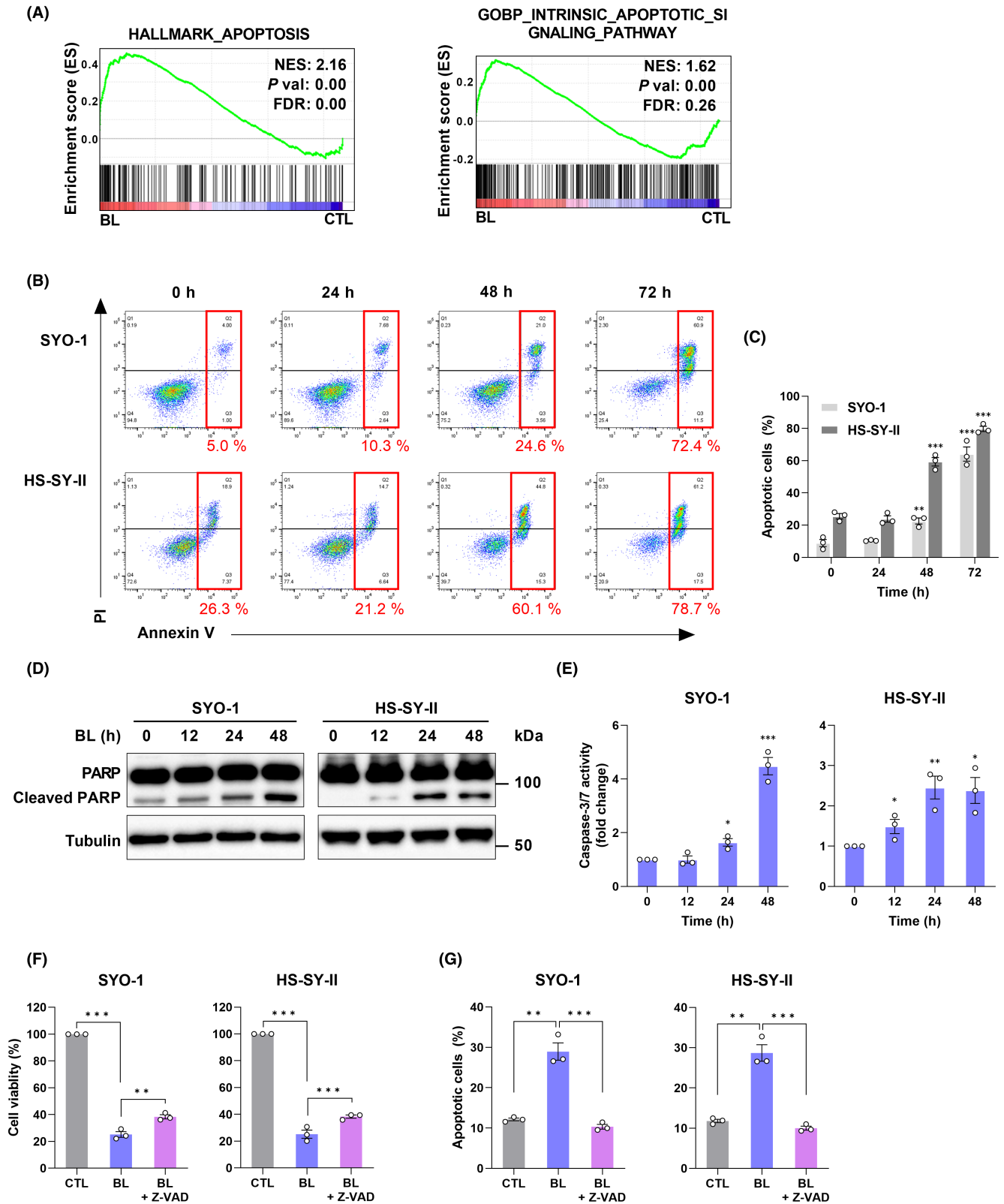


FIGURE 3 Blue light (BL) induced apoptosis in synovial sarcoma (SS) cells. (A) Gene set enrichment analysis (GSEA) of microarray data. NES, normalized enrichment score; FDR, false discovery rate. (B, C) The ratio of apoptotic cells was measured and analyzed by Annexin V-FITC/PI staining and flow cytometry (FC). (D) Caspase-3/7 activity was measured by CellEvent staining and FC. (E) Western blot analysis of PARP and cleaved PARP. (F) The CCK-8 assay was used to measure the cell viability of BL-irradiated SS cells in the presence or absence of a pan-caspase inhibitor, Z-VAD-FMK (Z-VAD, 100 μ M). (G) The ratio of apoptotic cells was measured and analyzed by Annexin V-FITC/PI staining and FC. Data are presented as the mean \pm SEM of three independent experiments. * p < 0.05, ** p < 0.01, *** p < 0.001. The quantification of western blot bands is presented in [Figure S7A](#).

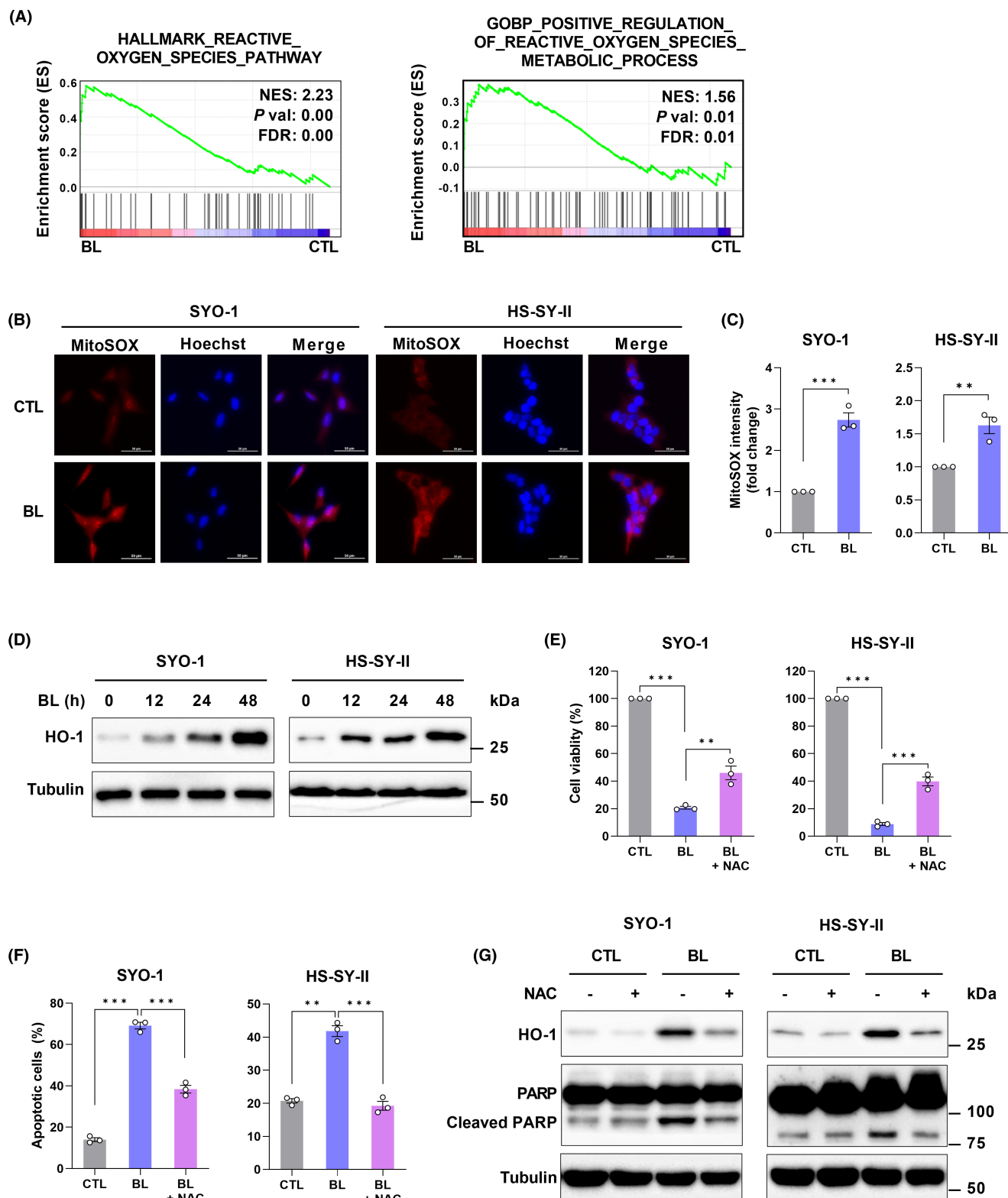


FIGURE 4 ROS are critical in BL-induced apoptosis in synovial sarcoma (SS) cells. (A) GSEA of microarray data. NES, normalized enrichment score; FDR, false discovery rate. (B) The production of mitochondrial ROS was assessed using a MitoSOX assay. Representative images of MitoSOX-stained cells captured by fluorescent microscopy are shown. (C) Quantification of mitochondrial ROS (MitoSOX) was measured by flow cytometry (FC). (D) The protein level of HO-1 was determined by western blotting. (E) The CCK-8 assay was used to measure the cell viability of BL-irradiated SS cells in the presence or absence of the ROS scavenger, N-acetyl-cysteine (NAC, 5 mM). (F) The ratio of apoptotic cells was measured and analyzed by Annexin V-FITC/PI staining and FC. (G) Western blot analysis of HO-1, PARP, and cleaved PARP. Data are presented as the mean \pm SEM of three independent experiments. * $p < 0.05$, ** $p < 0.01$, *** $p < 0.001$. The quantification of western blot bands is presented in Figure S7B-D.

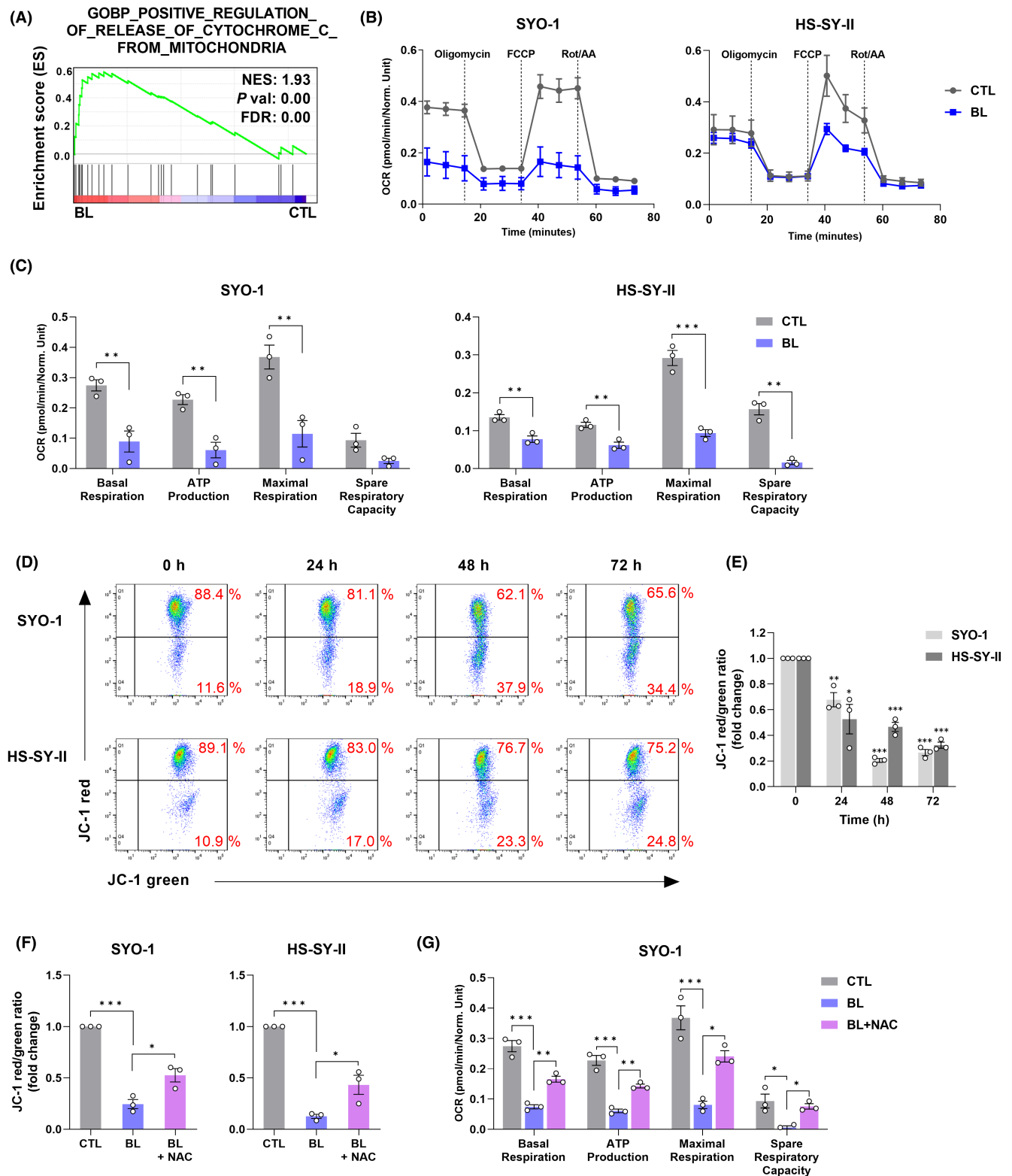


FIGURE 5 Blue light (BL) induced ROS production, thereby triggering mitochondrial dysfunction. (A) GSEA of microarray data. NES, normalized enrichment score; FDR, false discovery rate. (B) The OCR was measured with the Seahorse XF Cell Mito Stress assay using the Seahorse XF HS Mini analyzer. (C) Quantification of metabolic parameters. (D, E) The change in mitochondrial membrane potential (MMP) was measured by JC-1 and flow cytometry. (F) The MMP of BL-irradiated SS cells was measured by JC-1 in the presence or absence of NAC (5 mM). The data are presented as the mean \pm SEM of three independent experiments. * $p < 0.05$, ** $p < 0.01$, *** $p < 0.001$.

and spare respiratory capacity in SYO-1 and HS-SY-II cells (Figure 5B,C). Then the change in mitochondrial membrane potential (MMP), an important factor in mitochondrial dysfunction, was measured with JC-1 staining by flow cytometry. When mitochondria are healthy, JC-1 forms aggregates and emits red fluorescence, but when the MMP is reduced, JC-1 becomes monomeric and emits green fluorescence. Therefore, the ratio of red to green fluorescence is used as an indicator of mitochondrial damage. We observed a time-dependent decrease in the ratio of red/green fluorescence induced by BL (0.6 mW/cm²) (Figure 5D,E). These results indicated that BL induced severe damage in the mitochondria of SS cells.

Increased ROS might interfere with the MMP and electron transport chain for ATP synthase, upsetting the balance of energy homeostasis and causing cell death.^{32,33} Hence, to further analyze the link between ROS and mitochondrial dysfunction, SS cells were irradiated with BL (0.6 mW/cm²) with or without NAC (5 mM) for 48 h. Notably, the loss of MMP was remarkably reversed in the presence of NAC (Figure 5F,G). These results demonstrate that ROS generated by BL were responsible for the mitochondrial dysfunction.

3.6 | Autophagy occurs in response to BL-induced ROS and promotes SS cell survival

Autophagy-related signatures were enriched (Figure 6A); therefore, we determined whether autophagy was activated by BL. The CYTO-ID fluorescent probe specifically labeling autophagosomes in live cells was used. The results revealed that BL irradiation (0.6 mW/cm²) for 48 h stimulated the formation of autophagosomes in SYO-1 and HS-SY-II cells (Figure 6B), and flow cytometry analysis further confirmed these time-dependent findings (Figure 6C). Furthermore, the conversion of LC3-I to LC3-II, which are the major molecular players in autophagy signaling, was measured. As shown in Figure 6D, BL (0.6 mW/cm²) increased the accumulation of LC3B-II in SYO-1 and HS-SY-II cells. These results indicated that BL induced autophagy in SS cells.

ROS is well-known as a signaling molecule in the regulation of autophagy³⁴; therefore, the present study assessed whether ROS participated in BL-induced autophagy in SS cells. Predictably, inhibition of ROS by NAC (5 mM) attenuated the formation of autophagosomes (Figure 6E) and the expression of LC3B-II in SS cells (Figure 6F) induced by BL, suggesting that BL-induced autophagy was mediated by ROS accumulation in SS cells. The close and complex interplay between apoptosis and autophagy has been

demonstrated by the results of numerous evidence-based studies.³⁵ To clarify the interplay between autophagy and apoptosis in SS cells, we used 3-methyladenine (3-MA) to inhibit autophagy under BL irradiation. The CCK-8 and Annexin V-FITC/PI assays showed that BL in combination with 3-MA (5 mM) remarkably enhanced the effects of BL on cell viability (Figure S4) and apoptotic cell death (Figure 6G,H). We confirmed the results using western blotting and showed that SYO-1 cells irradiated with BL in the presence of 3-MA increased the levels of cleaved PARP (Figure 6I). To further confirm the connection between autophagy and apoptosis, specific siRNA against LC3B was applied. Knockdown of LC3B promoted inhibition of cell growth (Figure 6J) and the expression of cleaved PARP (Figure 6K). Taken together, BL induced autophagy, which promoted the survival of SS cells.

3.7 | BL suppresses the growth of SS cells in vivo

Finally, we investigated the effect of BL on the in vivo growth of SS cells by subcutaneously injecting SYO-1 cells into BALB/c nude mice. One week after injection, the mice were irradiated with BL (30 mW/cm², 8 h/day) for 12 days (Figure 7A,B). BL significantly inhibited tumor growth (Figure 7C), whereas the body weights of the mice in the CTL or BL group remained equal (Figure S5). The excised tumors showed that BL-induced tumors were much smaller than those of the CTL group (Figure 7D). The average weight of tumors in the BL group (360 ± 60 mg) was significantly lower than that of the CTL group (1002 ± 292 mg) (Figure 7E). After the mice were sacrificed, tumors were removed and Western blotting was performed. The results showed that the expression of apoptosis-related proteins (cleaved PARP and cleaved caspase-3) was increased in the BL group (Figure 7F,G), which is inconsistent with the in vitro findings. Moreover, BL-irradiated tumor tissues showed significant increases in TUNEL-positive cells and cleaved caspase-3 as well as a decrease in Ki-67-positive cells (Figure 7H,I). In addition, H&E staining of the skin above the tumor was performed to investigate the effect of BL on the skin tissue at the site of BL irradiation. No obvious skin damage due to BL irradiation was observed (Figure S6). These data suggest that BL exhibited a potent antitumor effect on SS in vivo that is safe with no side effects on normal tissues.

4 | DISCUSSION

In this study, we demonstrated that BL has a growth-inhibitory effect on SS cells and inhibits their migration

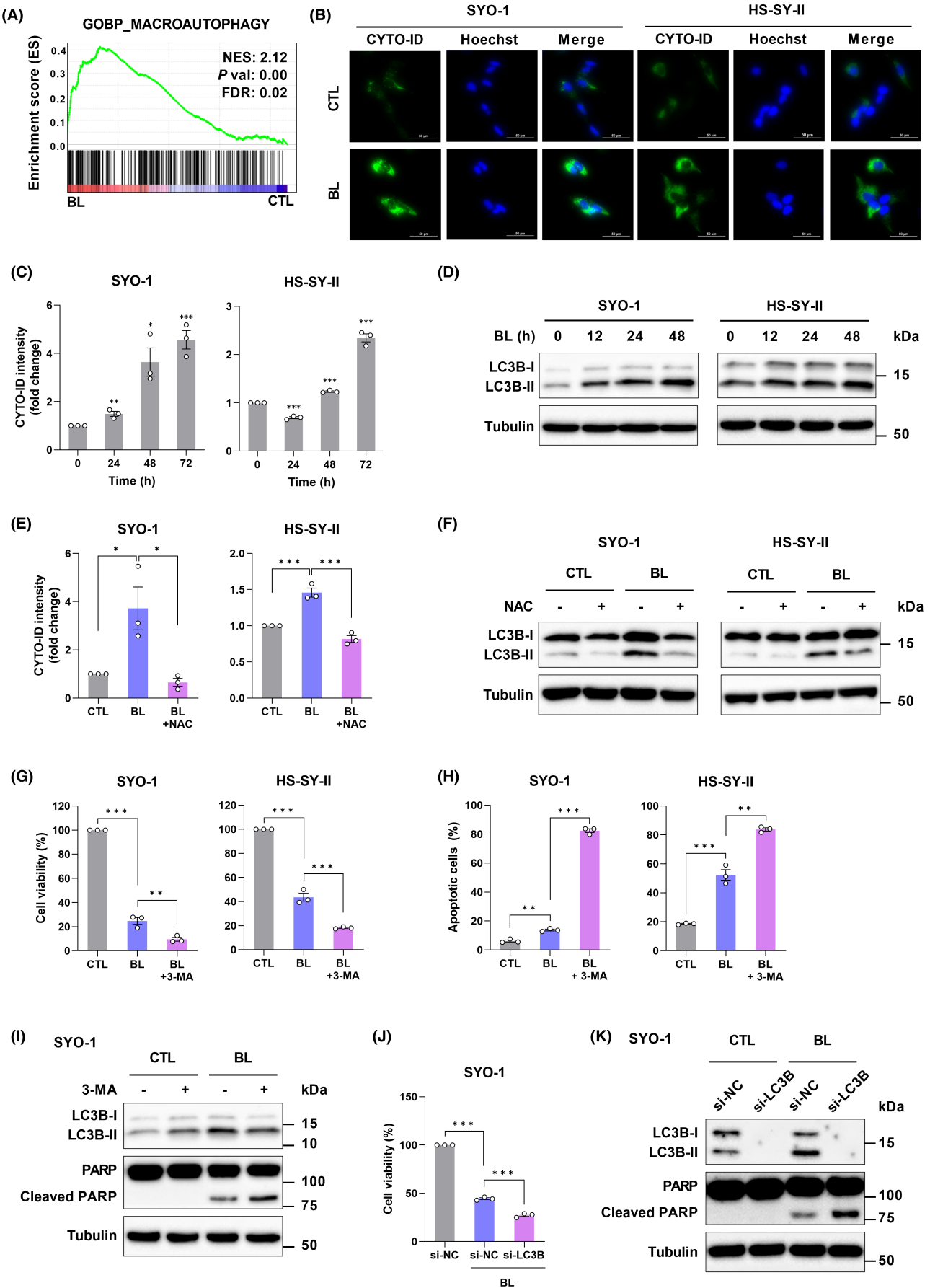


FIGURE 6 Legend on next page

FIGURE 6 Autophagy occurs in response to Blue light (BL)-induced ROS and promotes synovial sarcoma (SS) cell survival. (A) GSEA of microarray data. FDR, false discovery rate. (B) The formation of autophagosomes in SS cells was measured by CYTO-ID staining. Representative images of CYTO-ID-stained cells captured by fluorescent microscopy are shown. (C) Quantification of intracellular autophagosome (CYTO-ID) was measured by flow cytometry (FC). (D) Western blot analysis of LC3B-I and LC3B-II. (E) The formation of autophagosomes in BL-irradiated SS cells was assessed by CYTO-ID in the presence or absence of NAC (5 mM). (F) Western blot analysis of LC3B-I and LC3B-II. (G) The cell viability of BL-irradiated SS cells was assessed by the CCK-8 assay in the presence or absence of the autophagy inhibitor, 3-MA (5 mM). (H) The ratio of apoptotic cells was measured by Annexin V-FITC/PI staining and FC. Representative dot plot data are presented. (I) Western blot analysis of LC3B-I, LC3B-II, PARP, and cleaved PARP. (J) The cell viability of SYO-1 cells transfected with LC3B siRNA was measured by the CCK-8 assay. (K) Western blot analysis of LC3B-I, LC3B-II, PARP, and cleaved PARP. Data are presented as the mean \pm SEM of three independent experiments. * $p < 0.05$, ** $p < 0.01$, *** $p < 0.001$. The quantification of western blot bands is presented in Figure S7E–H.

and invasive ability. BL irradiation led to apoptosis through ROS-induced mitochondrial dysfunction, which caused the release of cytochrome c from mitochondria and induced apoptosis via the caspase pathway. Moreover, mitochondrial ROS accumulation induced autophagy, thereby inhibiting apoptosis and promoting cell survival. In addition, the inhibitory effect and safety of BL on SYO-1 xenograft models were demonstrated.

Mitochondria are said to contain chromophores such as cytochrome oxidase or flavin that absorb BL in the wavelength range of around 400–500 nm.^{36–38} When exposed to BL, chromophores become excited and react with intracellular oxygen molecules to generate singlet oxygen, which is one of the main ROS and is thought to cause mitochondrial dysfunction and damage to the respiratory chain complex. Excessive generation of mitochondrial ROS can lead to cell death. The fact that a growth-inhibitory effect on SS cells was observed only with BL and not with green and red light (Figure S1A) is considered to be due to the particular reaction of chromophores in mitochondria to BL.

The advantage of using BL as described in this paper is that it is less invasive than surgical treatment and is expected to cause less damage to the skin and other peritumor tissue compared with radiation therapy, because its wavelength is the visible light spectrum. Also, compared with chemotherapy, there are no systemic side effects. However, a possible adverse effect of BL on normal tissues is the generation of cytotoxic ROS in normal cells as well as SS cells, which causes oxidative damage to the cells. Nevertheless, it has been reported that cancer cells have higher ROS levels compared with normal cells and are able to delicately balance ROS with antioxidants in order to maintain their carcinogenic potential.³⁹ That is to say, cancer cells and normal cells differ in their cellular response to ROS, and cancer cells may be more inclined toward apoptosis resulting from an imbalance in the intracellular antioxidant system caused by excessive production of ROS, suggesting that BL might be applied to selectively target cancer cells. In this study, BL did not affect mouse skin tissue (Figure S6) but did have a growth-inhibitory

effect on HEK293 (Figure S1B), a non-cancer cell line. This in vitro result does not necessarily reflect the adverse effects of BL on normal tissues because the cell line is an immortalized cell that has undergone an extreme increase in proliferative capacity due to transformation and is not, strictly speaking, a normal cell.

This study identified autophagy inhibitors as candidate agents that enhance the anti-tumor effects of BL on SS. In cancer therapy research, autophagy has been reported to act on either cell survival or cell death.⁴⁰ Autophagic cell death has been reported in previous in vitro studies on the antitumor effects of BL on colon cancer cells¹⁴ and osteosarcoma cells.¹⁸ In the present study, we demonstrated that, in contrast to those reports, BL-induced autophagy is responsible for cell survival in SS (Figure 6G–K). Furthermore, we showed that 3-MA, an autophagy inhibitor, enhances the BL-induced apoptosis in SS cells (Figure 6G–I). These results suggest that autophagy inhibitors such as 3-MA might be used as sensitizers of BL. However, given that we have only been able to verify this in vitro, future studies on the in vivo antitumor-enhancing effects of autophagy inhibitors on BL are needed.

We also found that continuous irradiation of SS cells with a very low-power BL source showed marked antitumor effects. All previous studies that we have been able to find used high-power BL irradiation for 30 min to 24 h to investigate the effects on cancer cells.^{9–22} The concept of our study, with an eye toward initial clinical application, was to implant small wireless LEDs in the body and continuously irradiate the tumor. Therefore, it was necessary to develop an experimental model in which BL was irradiated at the lowest possible power for a long period of time, for example, up to 72 h. Recent studies have reported remarkable progress in the development of small wireless LEDs, and data from mouse animal experiments using small wireless LEDs in the fields of photodynamic therapy⁴¹ and photoimmunotherapy⁴² suggest the potential for these devices in BL therapy applications. If treatment involving BL irradiation of soft-tissue sarcomas using small wireless LEDs becomes feasible, it would provide a minimally invasive local adjuvant therapy with fewer side

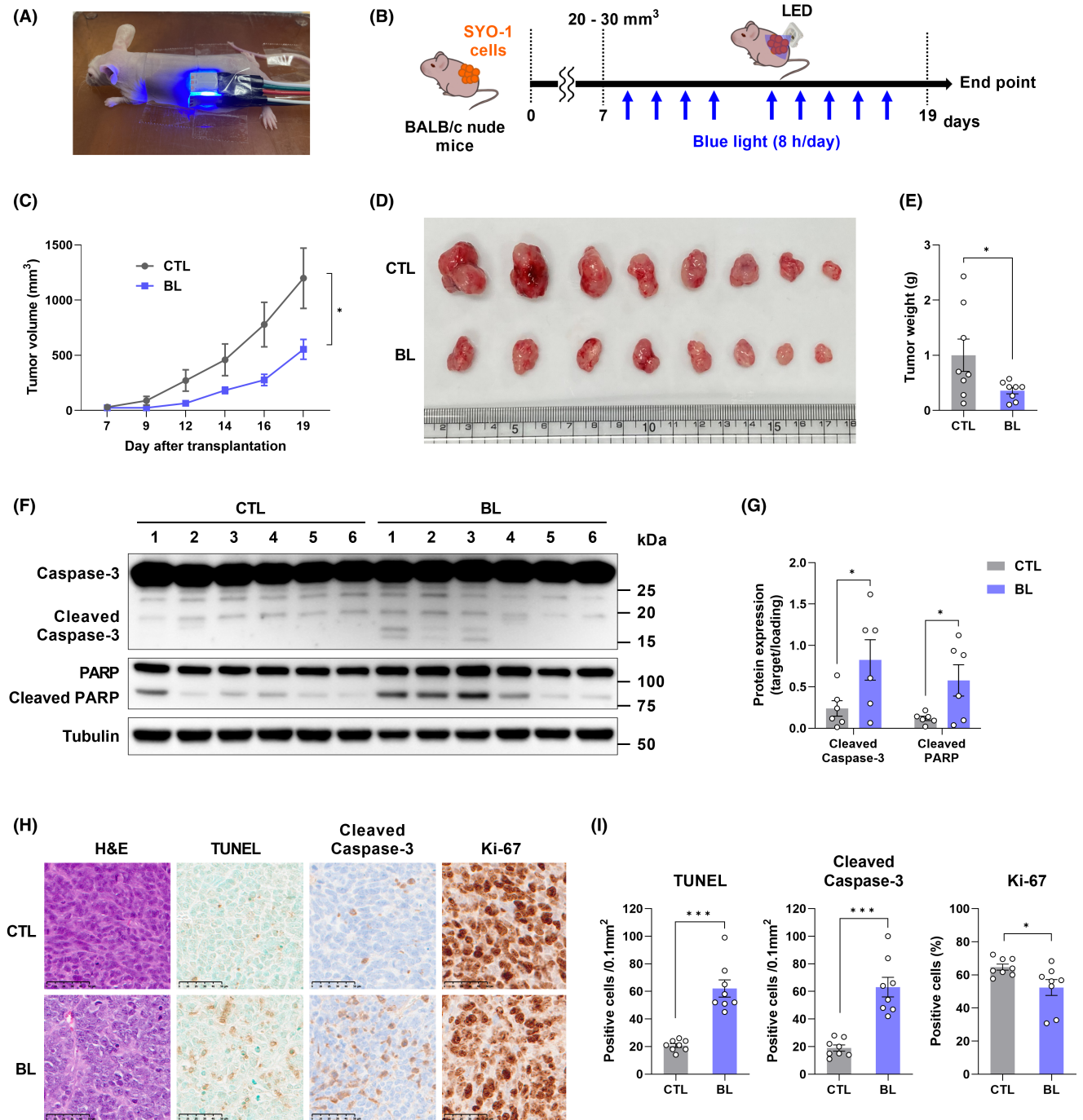


FIGURE 7 Blue light (BL) suppresses the growth of synovial sarcoma (SS) in vivo. (A) Image of BL irradiation in SYO-1 tumor-bearing nude mice. (B) Schematic illustration of the experimental protocol in vivo. (C) Tumor volumes in BALB/c nude mice during the 12-day BL irradiation. (D) Images of SYO-1 cells xenograft tumors at the end of the BL irradiation. (E) The weight of SYO-1 cell xenograft tumor at the end of the treatment. (F) Western blot analysis of the resected xenograft tumor. (G) Quantification of the protein expression is presented. (H) H&E staining was used to evaluate the histology. The apoptotic status of tumor tissues was assessed by the TUNEL assay. The expression of cleaved caspase-3 and Ki-67 was also examined by immunohistochemistry. (I) Quantification of TUNEL- and cleaved caspase-3-positive cells per field, and the percentage of Ki-67-positive cells. Data are presented as the mean \pm SEM. * $p < 0.05$, *** $p < 0.001$.

effects compared with conventional chemotherapy or radiation therapy.

We consider there to be two main limitations of this study. First, the in vivo studies did not confirm the

occurrence of BL-induced autophagy in SS, which was demonstrated in the in vitro studies. It is therefore necessary to confirm the protein expression levels of LC3 by Western blotting or tissue immunostaining, as was

performed in the verification of apoptosis. We have not yet been able to verify autophagy because we could not obtain sufficient amounts of tumor proteins or suitable antibodies for tissue immunostaining. We first need to verify BL-induced autophagy in vivo in order to use autophagy inhibitors as sensitizers for BL, as described above. Second, we have not yet been able to examine the depth to which BL penetrates and exerts its antitumor effects on the CAM tumors and mouse-transplanted tumors used in this study. As is generally known, BL has a shorter wavelength compared with red and near-infrared light and thus has lower tissue permeability.⁴³ If a tumor is larger than those transplanted in the mice in this study, BL might not be effective in shrinking the tumor due to its poor penetrability. We therefore need to conduct further experiments using rats or pigs to create larger tumors, investigate the permeability of BL in the tissues of these tumors, and further examine the potential clinical application of BL.

In conclusion, we analyzed in detail the antitumor effects of low-power continuous irradiation of BL on SS in vitro and in vivo. The results suggest the potential for BL irradiation to be applied in novel, minimally invasive therapies for the treatment of soft tissue sarcomas, including SS. In addition, with the advancement of LED technology, it may be possible to overcome the poor tissue permeability of BL by placing the light source near the tumor and performing continuous low-power irradiation that does not damage normal tissue as well as to enhance the effect of BL via combination with an autophagy inhibitor.

AUTHOR CONTRIBUTIONS

Makoto Takeuchi: Conceptualization (lead); data curation (lead); formal analysis (lead); investigation (lead); methodology (lead); software (lead); validation (lead); writing – original draft (lead). **Toshihiko Nishisho:** Conceptualization (equal); formal analysis (equal); project administration (lead); writing – review and editing (lead). **Shunichi Toki:** Data curation (equal); project administration (equal); visualization (equal); writing – review and editing (equal). **Shinji Kawaguchi:** Data curation (equal); investigation (equal); visualization (equal). **Shunsuke Tamaki:** Data curation (equal); investigation (equal). **Takeshi Oya:** Conceptualization (equal); data curation (equal); investigation (equal); supervision (equal); writing – review and editing (equal). **Yoshihiro Uto:** Formal analysis (supporting); methodology (equal); writing – review and editing (supporting). **Toyomasa Katagiri:** Supervision (supporting); writing – review and editing (supporting). **Koichi Sairyō:** Funding acquisition (lead); project administration (equal); resources (lead); supervision (lead).

ACKNOWLEDGMENTS

We are grateful to Drs. Masatake Akutagawa (Department of Electrical and Electronic Engineering, Division of Science and Technology, Graduate School of Technology, Industrial and Social Sciences, Tokushima University) and Koichiro Tsuchiya (Department of Medical Pharmacology, Institute of Biomedical Sciences, Tokushima University Graduate School) for technical support, helpful discussions, and comments on our study. This research was partially assisted by the Support Center for Advanced Medical Sciences, Tokushima University Graduate School of Biomedical Sciences, and partially supported by a grant from the Japan Orthopedics and Traumatology Research Foundation (No. 520).

CONFLICT OF INTEREST STATEMENT

The authors have no conflict of interest.

DATA AVAILABILITY STATEMENT

The data used in this study are available from the corresponding author upon reasonable request.

ETHICAL APPROVAL STATEMENT

Patients with synovial sarcoma provided informed consent before surgery for a portion of their resection specimens to be used for research. All experiments involving patient samples were performed after obtaining approval from the ethics committee of Tokushima University Hospital (Approval No. 1992–8). All animal experiments were conducted with approval from the Ethics Committee of Tokushima University for Animal Research (Approval No. T2021-64).

ORCID

Makoto Takeuchi  <https://orcid.org/0000-0003-2856-0264>

Shunichi Toki  <https://orcid.org/0000-0002-2546-6646>

REFERENCES

1. Fisher C. Synovial sarcoma. *Ann Diagn Pathol.* 1998;2:401-421.
2. Spillane AJ, A'Hern R, Judson IR, Fisher C, Thomas JM. Synovial sarcoma: a clinicopathologic, staging, and prognostic assessment. *J Clin Oncol.* 2000;18:3794-3803.
3. Lewis JJ, Antonescu CR, Leung DHY, et al. Synovial sarcoma: a multivariate analysis of prognostic factors in 112 patients with primary localized tumors of the extremity. *J Clin Oncol.* 2000;18:2087-2094.
4. Ashkenazi H, Malik Z, Harth Y, Nitzan Y. Eradication of *Propionibacterium acnes* by its endogenous porphyrins after illumination with high intensity blue light. *FEMS Immunol Med Microbiol.* 2003;35:17-24.
5. Trelles MA, Allones I. Red light-emitting diode (LED) therapy accelerates wound healing post-blepharoplasty and

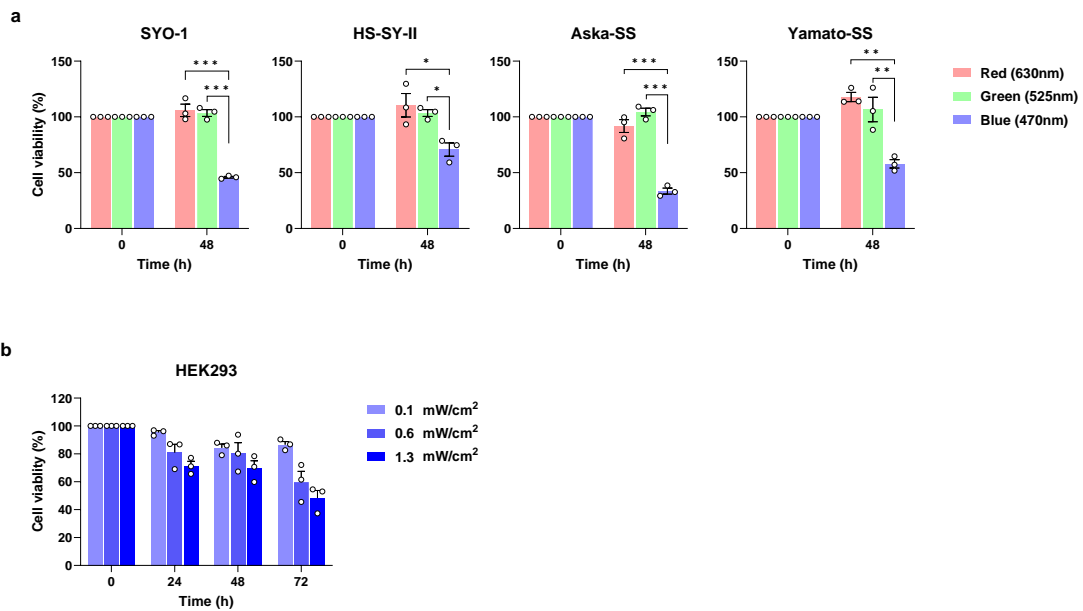
- periocular laser ablative resurfacing. *J Cosmet Laser Ther.* 2006;8:39-42.
6. Van Kets V, Karsten A, Davids LM. Laser light activation of a second-generation photosensitizer and its use as a potential photomodulatory agent in skin rejuvenation. *Lasers Med Sci.* 2013;28:589-595.
 7. Dai T, Gupta A, Murray CK, Vrahas MS, Tegos GP, Hamblin MR. Blue light for infectious diseases: Propionibacterium acnes, Helicobacter pylori, and beyond? *Drug Resist Updat.* 2012;15:223-236.
 8. Minamikawa T, Koma T, Suzuki A, et al. Publisher correction: quantitative evaluation of SARS-CoV-2 inactivation using a deep ultraviolet light-emitting diode. *Sci Rep.* 2021;11:16221.
 9. Ohara M, Kawashima Y, Katoh O, Watanabe H. Blue light inhibits the growth of B16 melanoma cells. *Jpn J Cancer Res.* 2002;93:551-558.
 10. Sato K, Minai Y, Watanabe H. Effect of monochromatic visible light on intracellular superoxide anion production and mitochondrial membrane potential of B16F1 and B16F10 murine melanoma cells. *Cell Biol Int.* 2013;37:633-637.
 11. Oh PS, Hwang H, Jeong HS, et al. Blue light emitting diode induces apoptosis in lymphoid cells by stimulating autophagy. *Int J Biochem Cell Biol.* 2016;70:13-22.
 12. Matsumoto N, Yoshikawa K, Shimada M, et al. Effect of light irradiation by light emitting diode on colon cancer cells. *Anticancer Res.* 2014;34:4709-4716.
 13. Oh PS, Kim HS, Kim EM, et al. Inhibitory effect of blue light emitting diode on migration and invasion of cancer cells. *J Cell Physiol.* 2017;232:3444-3453.
 14. Yoshimoto T, Morine Y, Takasu C, et al. Blue light-emitting diodes induce autophagy in colon cancer cells by Opsin 3. *Ann Gastroenterol Surg.* 2018;2:154-161.
 15. Yoshimoto T, Shimada M, Tokunaga T, et al. Blue light irradiation inhibits the growth of colon cancer and activation of cancer-associated fibroblasts. *Oncol Rep.* 2022;47:104.
 16. Zhuang J, Liu Y, Yuan Q, et al. Blue light-induced apoptosis of human promyelocytic leukemia cells via the mitochondrial-mediated signaling pathway. *Oncol Lett.* 2018;15:6291-6296.
 17. Kim YM, Ko SH, Shin YI, et al. Light-emitting diode irradiation induces AKT/mTOR-mediated apoptosis in human pancreatic cancer cells and xenograft mouse model. *J Cell Physiol.* 2021;236:1362-1374.
 18. He M, Yan G, Wang Y, et al. Blue LED causes autophagic cell death in human osteosarcoma by increasing ROS generation and dephosphorylating EGFR. *J Cell Mol Med.* 2021;25:4962-4973.
 19. Ohara M, Fujikura T, Fujiwara H. Augmentation of the inhibitory effect of blue light on the growth of B16 melanoma cells by riboflavin. *Int J Oncol.* 2003;22:1291-1295.
 20. Yan G, Zhang L, Feng C, et al. Blue light emitting diodes irradiation causes cell death in colorectal cancer by inducing ROS production and DNA damage. *Int J Biochem Cell Biol.* 2018;103:81-88.
 21. Zhuang J, Xia L, Zou Z, Yin J. Blue light induces ROS mediated apoptosis and degradation of AML1-ETO oncoprotein in Kasumi-1 cells. *Med Oncol.* 2022;39:52.
 22. Oh PS, Na KS, Hwang H, et al. Effect of blue light emitting diodes on melanoma cells: involvement of apoptotic signaling. *J Photochem Photobiol B.* 2015;142:197-203.
 23. Kawai A, Naito N, Yoshida A, et al. Establishment and characterization of a biphasic synovial sarcoma cell line, SYO-1. *Cancer Lett.* 2004;204:105-113.
 24. Freshney R. *Culture of Animal Cells: A Manual of Basic Technique.* Alan R. Liss, Inc; 1987.
 25. Oyewole AO, Birch-Machin MA. Mitochondria-targeted antioxidants. *FASEB J.* 2015;29:4766-4771.
 26. Furfaro AL, Traverso N, Domenicotti C, et al. The Nrf2/HO-1 axis in cancer cell growth and chemoresistance. *Oxid Med Cell Longev.* 2016;2016:1958174.
 27. Tsai CH, Shen YC, Chen HW, et al. Docosahexaenoic acid increases the expression of oxidative stress-induced growth inhibitor 1 through the PI3K/Akt/Nrf2 signaling pathway in breast cancer cells. *Food Chem Toxicol.* 2017;108:276-288.
 28. Oh ET, Park HJ. Implications of NQO1 in cancer therapy. *BMB Rep.* 2015;48:609-617.
 29. Bonelli M, Savitskaya A, Steiner CW, et al. Heme oxygenase-1 end-products carbon monoxide and biliverdin ameliorate murine collagen induced arthritis. *Clin Exp Rheumatol.* 2012;30:73-78.
 30. Yu ZY, Ma D, He ZC, et al. Heme oxygenase-1 protects bone marrow mesenchymal stem cells from iron overload through decreasing reactive oxygen species and promoting IL-10 generation. *Exp Cell Res.* 2018;362:28-42.
 31. Hajra KM, Liu JR. Apoptosome dysfunction in human cancer. *Apoptosis.* 2004;9:691-704.
 32. Almada M, Fonseca BM, Amaral C, Diniz-da-Costa M, Correia-da-Silva G, Teixeira N. Anandamide oxidative metabolism-induced endoplasmic reticulum stress and apoptosis. *Apoptosis.* 2017;22:816-826.
 33. Zhang BB, Wang DG, Guo FF, Xuan C. Mitochondrial membrane potential and reactive oxygen species in cancer stem cells. *Fam Cancer.* 2015;14:19-23.
 34. Li L, Tan J, Miao Y, Lei P, Zhang Q. ROS and autophagy: interactions and molecular regulatory mechanisms. *Cell Mol Neurobiol.* 2015;35:615-621.
 35. Eisenberg-Lerner A, Bialik S, Simon HU, Kimchi A. Life and death partners: apoptosis, autophagy and the cross-talk between them. *Cell Death Differ.* 2009;16:966-975.
 36. Vamecq J, Draye JP. Pathophysiology of peroxisomal beta-oxidation. *Essays Biochem.* 1989;24:115-225.
 37. Chen E, Söderberg PG, Lindström B. Cytochrome oxidase activity in rat retina after exposure to 404 nm blue light. *Curr Eye Res.* 1992;11:825-831.
 38. Lubart R, Wollman Y, Friedmann H, Rochkind S, Laulich I. Effects of visible and near-infrared lasers on cell cultures. *J Photochem Photobiol B.* 1992;28:305-310.
 39. Khan AQ, Rashid K, Al Amodi AA, et al. Reactive oxygen species (ROS) in cancer pathogenesis and therapy: an update on the role of ROS in anticancer action of benzophenanthridine alkaloids. *Biomed Pharmacother.* 2021;143:112142.
 40. Choi AM, Ryter SW, Levine B. Autophagy in human health and disease. *N Engl J Med.* 2013;368:651-662.
 41. Yamagishi K, Kirino I, Takahashi I, et al. Tissue-adhesive wirelessly powered optoelectronic device for metronomic photodynamic cancer therapy. *Nat Biomed Eng.* 2019;3:27-36.
 42. Nakajima K, Kimura T, Takakura H, et al. Implantable wireless powered light emitting diode (LED) for near-infrared photodynamic therapy: device development and experimental assessment in vitro and in vivo. *Oncotarget.* 2018;9:20048-20057.

43. Ash C, Dubec M, Donne K, Bashford T. Effect of wavelength and beam width on penetration in light-tissue interaction using computational methods. *Lasers Med Sci.* 2017;32:1909-1918.

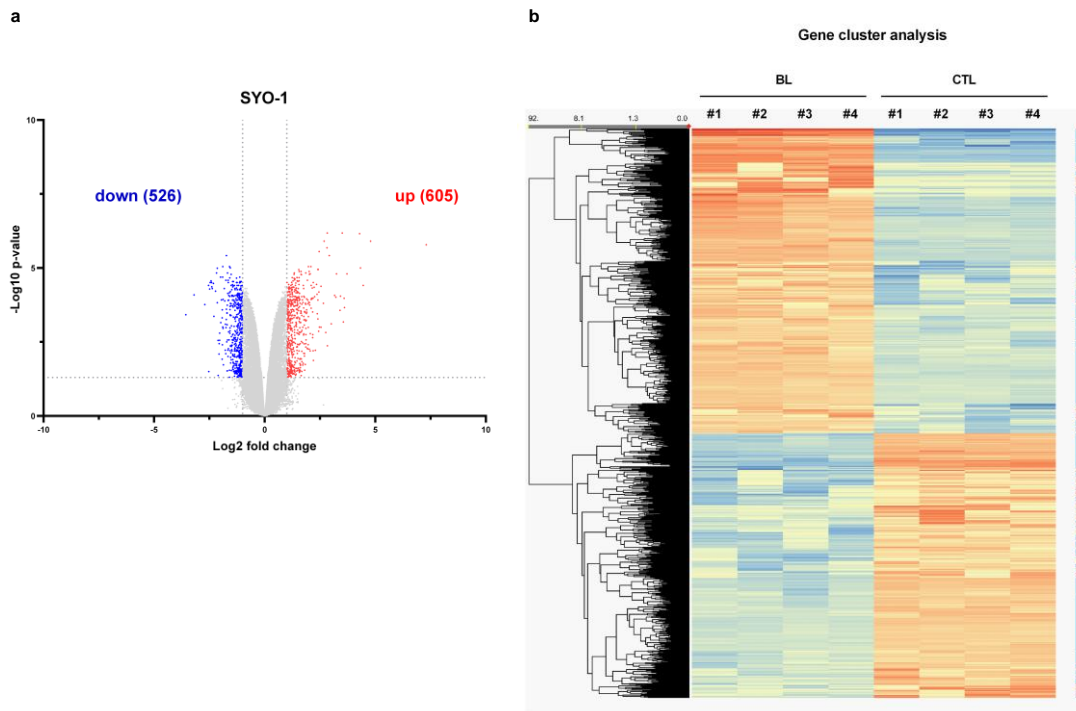
SUPPORTING INFORMATION

Additional supporting information can be found online in the Supporting Information section at the end of this article.

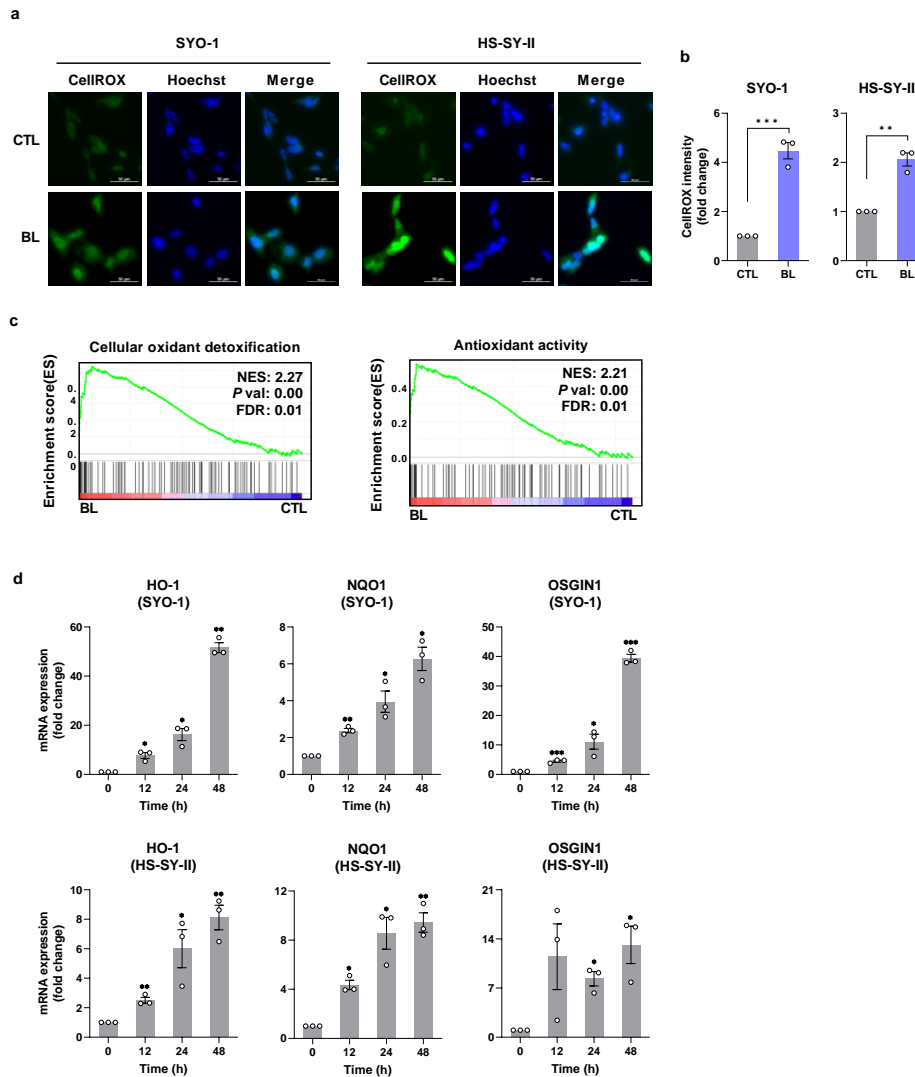
How to cite this article: Takeuchi M, Nishisho T, Toki S, et al. Blue light induces apoptosis and autophagy by promoting ROS-mediated mitochondrial dysfunction in synovial sarcoma. *Cancer Med.* 2023;00:1-16. doi:[10.1002/cam4.5664](https://doi.org/10.1002/cam4.5664)



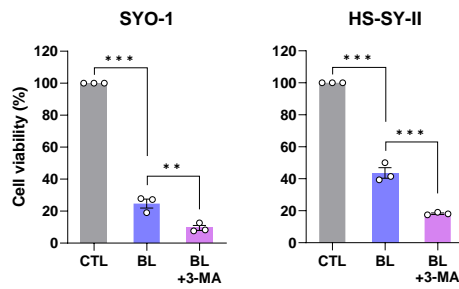
Supplementary Figure 1. (a) SS cells were irradiated with blue (peak at 470 nm), green (peak at 525 nm), or red (peak at 630 nm) light at a light intensity of 0.6 mW/cm² for 48 h, after which cell viability was measured with the CCK-8 assay. (b) Results of the CCK-8 assay. Data are presented as the mean \pm SEM of three independent experiments. * $P < 0.05$, ** $P < 0.01$, *** $P < 0.001$.



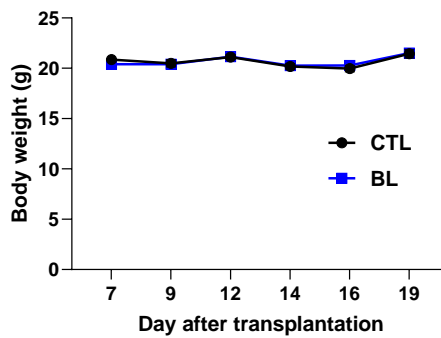
Supplementary Figure 2. (a) Volcano plot visualizing DEGs between the BL group, which was irradiated with BL (0.6 mW/cm²) for 48 h, and the control group in SYO-1 cells. Red dots (upregulated) and blue dots (downregulated) were defined as DEGs by cutoff log₂ (fold change) >1 and corrected *P* > 0.05, and gray dots indicate transcripts that did not change significantly between the two groups. (b) Gene cluster analysis (Euclidean distance, Ward-linked) of 1,131 DEGs with quadruplicate samples was conducted. The X-axis represents the DEGs and the Y-axis represents the samples.



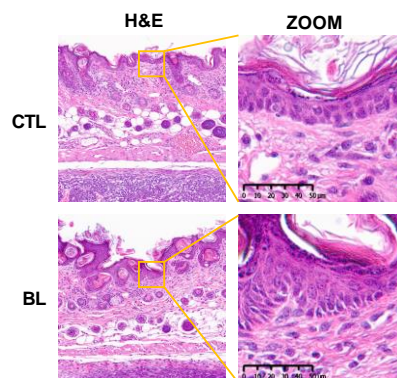
Supplementary Figure 3. (a) The production of intracellular ROS was assessed by the CellIROX assay. Representative images of CellIROX stained cells captured by fluorescent microscopy are shown. (b) Quantification of intracellular ROS (CellIROX) was measured by flow cytometry. (c) GSEA of microarray data. NES: normalized enrichment score; FDR: false discovery rate. (d) The mRNA expression of HO-1, NAD(P)H:quinone oxidoreductase 1 (NQO1), and oxidative stress induced growth inhibitor 1 (OSGIN1) was measured by qPCR. Data are presented as the mean \pm SEM of three independent experiments. $**P < 0.01$, $***P < 0.001$.



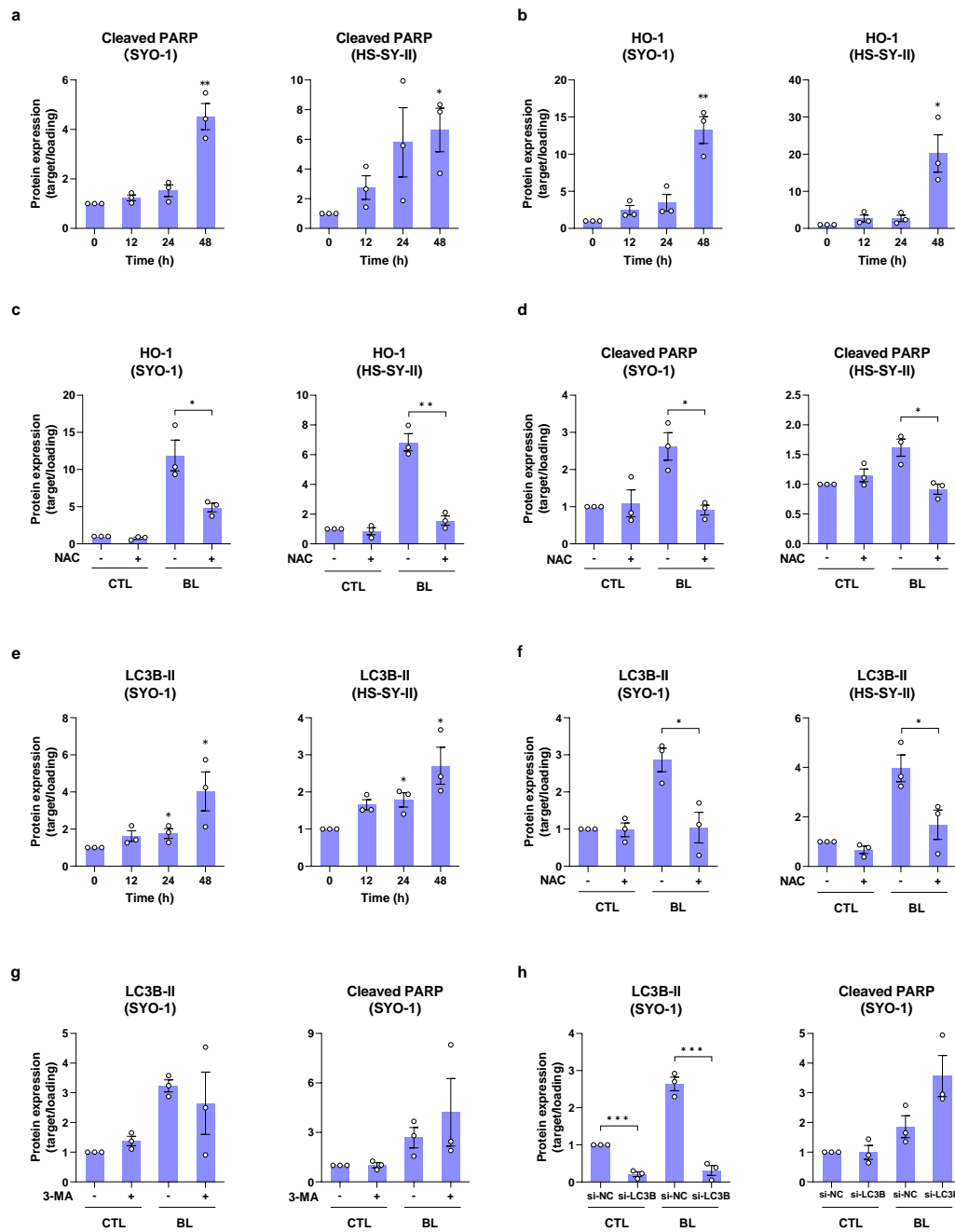
Supplementary Figure 4. SYO-1 and HS-SY-II cells were irradiated with BL (0.6 mW/cm²) for 48 h in the presence or absence of the autophagy inhibitor 3-MA (5 mM), after which cell viability was assessed by the CCK-8 assay.



Supplementary Figure 5. Mice body weight were recorded and compared. Data are presented as the mean \pm SEM.



Supplementary Figure 6. H&E staining of mouse skin tissue directly above the transplanted tumor was performed to investigate the effect of BL on the skin tissue.



Supplementary Figure 7. Quantification of western blot bands in the main figures. (a, b, e) SYO-1 and HS-SY-II cells were irradiated with BL (0.6 mW/cm²) for the indicated times. (c, d, f) SYO-1 and HS-SY-II cells were irradiated with BL (0.6 mW/cm²) with or without N-acetyl-cysteine (NAC, 5 mM). (g) SYO-1 cells were irradiated with BL (0.6 mW/cm²) with or without 3-methyladenine (3-MA, 5 mM). (h) SYO-1 cells were irradiated with BL (0.6 mW/cm²) after si-NC or si-LC3B treatment. Data are presented as the mean \pm SEM of three independent experiments. * P < 0.05, ** P < 0.01, *** P < 0.001.

Supplementary Materials and Methods

Cell viability assay

Cell viability was determined using the Cell Counting Kit-8 (CCK-8; Dojindo) according to the manufacturer's protocol. The cells were seeded in 96-well plates at a density of 1×10^4 cells per well, incubated overnight until attachment, and exposed to light with various light intensities for the indicated time periods. Then the medium was replaced with 100 μ L medium containing 10 μ L CCK-8, and the cells were incubated for 1–4 h. The absorbance was measured at 450 nm with a microplate reader (Varioskan Flash; Thermo Fisher Scientific).

Colony formation assay

Cells were seeded in 6-well plates at a density of 1×10^3 cells per well. The cells were irradiated with BL (0.1 mW/cm²) for 24 h. Then the cells were cultured continuously for 14 days. Finally, the cells were fixed in 100% methanol, stained with 0.5% crystal violet (Sigma-Aldrich) in 20% methanol, and photographed.

Wound healing assay

Cells were seeded on a culture-insert (ibidi culture-insert 2 well; ibidi GmbH) at a density of 5×10^5 cells/mL. After allowing the cells to attach overnight, the culture-insert was removed, followed by BL irradiation (0.6 mW/cm²). Wound areas were photographed at the indicated times, and the wound healing rate was calculated under a light microscope (Nikon). Healing rate = (width of the wound at \times h – width of the wound at 0 h)/width of the wound at 0 h.

Transwell migration and invasion assay

Filter inserts that fit into 24-well chambers (Corning) were used for the migration assay. The

cells were seeded in the upper chamber at a density of 1×10^5 cells/0.5 mL in serum-free medium. Then, 0.75 mL 10% FBS-supplemented medium was added to the lower chamber. After irradiation with BL, the non-migrating cells were gently removed from the surface of the chamber with cotton swabs. Next, the migrating cells on the chamber bottom were fixed and stained using Diff-Quik solutions (Sysmex). After the filter was dried, the invaded cells were imaged and counted under a light microscope. In the invasion assay, the cells were seeded in the Matrigel-coated inserts (Corning) at a density of 1×10^5 cells/0.5 mL and allowed to invade under BL irradiation. The invasive cells were subsequently stained and analyzed as described above.

Microarray analysis

The total RNA of SYO-1 cells incubated with or without BL irradiation (0.6 mW/cm^2) for 48 h was extracted using the RNeasy kit (Qiagen) from quadruplicate samples. The RNA samples were labeled with cyanine-3 (cRNA) using the Low Input Quick Amp Labeling Kit (Agilent Technologies). The cRNAs were applied to the slides and analyzed on the SurePrint G3 Human GE Microarray 8×60 K (Agilent Technologies). Quantile normalization and the creation of a cluster heat map were performed using GeneSpring GX software (Agilent Technologies). The volcano plot and bubble plot were made by GraphPad Prism 9 (GraphPad Software). The sample data file was imported into gene set enrichment analysis (GSEA) software (<https://www.gsea-msigdb.org/gsea/index.jsp>).

Apoptosis assay

Dead Cell Apoptosis Kits with Annexin V for Flow Cytometry (Thermo Fisher Scientific) were used to measure cell apoptosis. Briefly, cells were plated in a 6-well plate at a density of $1 \times$

10⁵ cells per well and irradiated with BL (0.6 mW/cm²) for the indicated times. Then the cells were harvested and washed twice with PBS. The cells were incubated with Annexin V-FITC and propidium iodide (PI) for 15 min in the dark at room temperature, and stained apoptotic cells were counted with flow cytometry (FC; BD FACSVerse; Becton Dickinson).

Caspase activity assay

Caspase activation was studied using the CellEvent Caspase-3/7 detection reagent (Thermo Fisher Scientific). Cells were seeded in a 6-well plate at a density of 1 × 10⁵ cells per well, incubated overnight, and irradiated with BL (0.6 mW/cm²) for the indicated times. The cells were harvested, washed twice with PBS, and then incubated with CellEvent reagent for 30 min in the dark at 37°C. Finally, the cells were harvested and analyzed by FC.

Western blot analysis

Cells were harvested with a scraper and lysed in RIPA buffer supplemented with protease and phosphatase inhibitors (Thermo Fisher Scientific). After incubation on ice for 30 min, the lysates were centrifuged at 15,000 rpm for 15 min at 4°C, and then the supernatant was moved to a new tube for analysis of the protein concentrations by the BCA Protein Assay Kit (Takara, Shiga, Japan). Collected proteins were subjected to 8%, 10%, or 15% sodium dodecyl sulfate-polyacrylamide gel electrophoresis and transferred to 0.45 μm PVDF membranes (Millipore, MA). After blocking, the membranes were incubated with the following primary antibodies: poly (ADP-ribose) polymerase (PARP) (#9542; Cell Signaling Technology [CST]), heme oxygenase-1 (HO-1) (E3F4S, #43966; CST), light chain 3B (LC3B) (#2775; CST), caspase-3 (#9662; CST), and α/β tubulin (#2148; CST), all of them diluted 1:1000. The membranes were washed with Tris-buffered saline with 0.1% Tween buffer and incubated with diluted anti-rabbit IgG horseradish peroxidase-linked secondary antibody

(1:3000, #7074; CST). Blots were visualized using Amersham ECL Prime (Cytiva, Tokyo, Japan). The FUSION FX. EDGE System (Vilber Lourmat) was used for the imaging, and protein levels were based on the signal intensity.

Measurement of reactive oxygen species

The CellROX reagent (Thermo Fisher Scientific) for detecting intracellular (total) reactive oxygen species (ROS) and MitoSOX Red reagent (Thermo Fisher Scientific) for detecting mitochondrial ROS were used according to the manufacturer's instructions. Briefly, cells were seeded in a 6-well plate at 1.0×10^5 cells per well and incubated overnight with or without BL irradiation (0.6 mW/cm^2) for 48 h. The cells were treated with CellROX ($1 \text{ }\mu\text{M}$) for 1 h or MitoSOX ($5 \text{ }\mu\text{M}$) for 30 min and then harvested for FC.

Quantitative PCR analysis

Total RNA was extracted using the RNeasy kit (Qiagen). RNA from each sample was used to synthesize complementary DNA using the iScript cDNA Synthesis Kit (Bio-Rad) according to the manufacturer's protocol. For quantitative PCR (qPCR), we used the Power SYBR Green Master Mix (Thermo Fisher Scientific) and the results were normalized to 18S ribosomal RNA. The primers used are listed in Table S4.

Determination of the oxygen consumption rate

The oxygen consumption rate (OCR) was measured using the Seahorse XF Cell Mito Stress assay on the Seahorse XF HS Mini Analyzer (Agilent Technologies) according to the manufacturer's instructions. Briefly, cells were seeded and incubated overnight with or without BL irradiation. Before measurements, plates were equilibrated in a CO_2 -free

incubator at 37°C for 1 h. Analysis was performed using 1.5 µM oligomycin, 2.0 µM carbonyl cyanide-4-(trifluoromethoxy) phenylhydrazone, and 0.5 µM rotenone/antimycin A as indicated. Data were analyzed using the Seahorse XF Cell Mito Stress Test Report generator software (Agilent Technologies). Data were normalized to the actual cell count using Hoechst 33342 (Thermo Fisher Scientific) staining immediately after OCR recording.

Measurement of mitochondrial membrane potential

Mitochondrial membrane potential was measured using the JC-1 MitoMP Detection Kit (Dojindo) according to the manufacturer's protocol. In brief, cells were seeded in a 6-well plate at a density of 1.0×10^5 cells per well, incubated overnight, and irradiated with BL (0.6 mW/cm²) for the indicated times. Then, the cells were harvested, washed twice with PBS, and stained with JC-1 at 37°C for 30 min in the dark. Subsequently, stained cells were washed, resuspended, and subjected to FC.

Autophagy assay

The CYTO-ID Autophagy Detection Kit (Enzo Life Sciences) was used. Cells were seeded in a 6-well plate at a density of 1.0×10^5 cells per well, incubated overnight, and irradiated with BL (0.6 mW/cm²) for the indicated times. Then, the cells were collected and incubated with CYTO-ID detection reagent for autophagic vesicle staining at 37°C for 30 min in the dark. Subsequently, stained cells were washed, resuspended, and subjected to FC.

Small interfering RNA transfection

The Silencer Select Predesigned small interfering RNA (siRNA) (ID: s224886 for human LC3B) was purchased from Ambion. Negative control siRNA was purchased from Nippon

Gene. The si-LC3B (final concentration, 10 nM) was combined with Lipofectamine RNAiMAX Transfection Reagent (Thermo Fisher Scientific) and mixed for 15 min in each well, followed by the addition of suspension cells. The cells were incubated overnight and the medium was replaced with fresh one. The inhibition efficiency was detected by western blotting to confirm.

Histology and immunohistochemistry

Removed tissues were fixed in 4% paraformaldehyde for 48 h and embedded in paraffin blocks. Three-micron-thick sections were mounted on glass slides, deparaffinized, rehydrated, and stained with H&E using standard protocols. Immunohistochemistry was performed with an automated staining system using DAKO Autostainer Link48 (Agilent Technologies). Following pretreatment with the EnVision FLEX Target Retrieval Solution, High pH (Agilent Technologies), unstained 4 µm-thick sections were incubated with a rabbit monoclonal antibody against cleaved caspase-3 (Asp175) (1:500, clone 5A1E, #9664; CST) and a mouse monoclonal antibody against Ki-67 (1:100, clone MIB-1; Dako). Signals were detected using the Envision FLEX DAB+ (Agilent Technologies), and the sections were counterstained with Envision FLEX hematoxylin (Agilent Technologies).

TUNEL analysis

Apoptosis detection was identified using the ApopTag Plus Peroxidase In Situ Apoptosis Kit (Millipore) according to the manufacturer's instructions. Briefly, sections were initially incubated with the TdT enzyme, which links digoxigenin-dNTP to apoptotic DNA fragments. Anti-digoxigenin antibody conjugated with peroxidase was applied to detect the digoxigenin-dNTP tails.

Supplementary Table 1.

Clinicopathological data of the two patients with synovial sarcoma from whom the samples in this study were derived.

Patient	Age (y)	Sex	Location	Size (cm)	Distant metastasis	Stage	Neo adjuvant chemotherapy	Histology: subtype	IHC: SS18-SSX
P1	42	M	Chest wall	11.2	No	IIIB	AI (DXR + IFO)	Biphasic	Positive
P2	59	M	Ankle	7.5	No	IIIA	No	Poorly differentiated	Positive

y: year, M: male, DXR: doxorubicin, IFO: ifosfamide, IHC: immunohistochemistry

Supplementary Table 2. Reagents used in this study.

Reagents	Source	Catalog Number
Seahorse XF Cell Mito Stress Test Kit	Agilent Technologies (Santa Clara, CA)	103010-100
DMEM assay medium pack	Agilent Technologies (Santa Clara, CA)	103680-100
EnVision FLEX Target Retrieval Solution, High PH	Agilent Technologies (Santa Clara, CA)	K8004
EnVision FLEX DAB+	Agilent Technologies (Santa Clara, CA)	GV825
Envision FLEX hematoxylin	Agilent Technologies (Santa Clara, CA)	K8008
SurePrint G3 Human GE Microarray 8x60K Ver. 3.0	Agilent Technologies (Santa Clara, CA)	G4858A#72363
RNA Spike In Kit	Agilent Technologies (Santa Clara, CA)	5188-5282
Low Input Quick-Amp Labeling Kit	Agilent Technologies (Santa Clara, CA)	5190-2305
Gene Expression Hybridization Kit	Agilent Technologies (Santa Clara, CA)	5188-5242
GE Wash Pack	Agilent Technologies (Santa Clara, CA)	5188-5327
Silencer Select Pre-designed siRNA for human LC3B	Ambion (Grand Island, NY)	s224886
4x Laemmli Sample Buffer	Bio-Rad (Hercules, CA)	1610747
2-Mercaptoethanol	Bio-Rad (Hercules, CA)	1610710
10x Tris/Glycine/SDS	Bio-Rad (Hercules, CA)	1610732
10x Tris/Glycine	Bio-Rad (Hercules, CA)	1610734
10x TBS	Bio-Rad (Hercules, CA)	1706435
10% Tween 20	Bio-Rad (Hercules, CA)	1610781
30% Acrylamide/Bis Solution	Bio-Rad (Hercules, CA)	1610158
Resolving Gel Buffer for PAGE	Bio-Rad (Hercules, CA)	1610798
Stacking Gel Buffer for PAGE	Bio-Rad (Hercules, CA)	1610799
Ammonium Persulfate (APS)	Bio-Rad (Hercules, CA)	1610700
TEMED	Bio-Rad (Hercules, CA)	1610800
Precision Plus Protein Dual Color Standards	Bio-Rad (Hercules, CA)	1610374
Precision Plus Protein All Blue Prestained	Bio-Rad (Hercules, CA)	1610373
iScript Advanced cDNA Synthesis kit	Bio-Rad (Hercules, CA)	1725038
EvaGreen 20X in Water	Biotium (Fremont, CA)	31000
PARP Antibody	Cell Signaling Technology (Danvers, MA)	9542
HO-1 (E3F4S)	Cell Signaling Technology (Danvers, MA)	43966
LC3B Antibody	Cell Signaling Technology (Danvers, MA)	2775
Caspase-3 Antibody	Cell Signaling Technology (Danvers, MA)	9662
α/β -Tubulin Antibody	Cell Signaling Technology (Danvers, MA)	2148
Cleaved Caspase-3 (Asp175)	Cell Signaling Technology (Danvers, MA)	9664
Anti-rabbit IgG, HRP-linked Antibody	Cell Signaling Technology (Danvers, MA)	7074S
ECL Prime Western Blotting Detection Reagent	Cytiva (Tokyo, Japan)	RPN2232
Ki-67 Antigen	DAKO (Glostrup, Denmark)	M7240
Cell Counting Kit-8	Dojindo (Kumamoto, Japan)	341-07624
JC-1 MitoMP Detection Kit	Dojindo (Kumamoto, Japan)	MT09
CYTO-ID autophagy detection kit	Enzo Life Sciences (Farmingdale, NY)	ENZ-KIT175-0200
ApopTag Plus Peroxidase In Situ Apoptosis Kit	Millipore (Burlington, MA)	S7101
4%-Paraformaldehyde Phosphate Buffer Solution	Nakalai (Kyoto, Japan)	09154-56

Negative control siRNA	Nippon Gene (Tokyo, Japan)	211124
RNeasy Mini Kit (50)	QIAGEN (Hilden, Germany)	74104
Phosphate Buffered Saline	Santa Cruz Biotechnology (Santa Cruz, CA)	
3-Methyladenine	Selleckchem (Houston, TX)	5142-23-4
Dulbecco's Modified Eagle's Medium	Sigma-Aldrich (St.Louis, MO)	D6046
Fetal Bovine Serum	Sigma-Aldrich (St.Louis, MO)	F7524
Penicillin-Streptomycin	Sigma-Aldrich (St.Louis, MO)	D6046
Collagenase from Clostridium h	Sigma-Aldrich (St.Louis, MO)	C2139
Crystal violet solution	Sigma-Aldrich (St.Louis, MO)	V5265
N-Acetyl-L-cysteine	Sigma-Aldrich (St.Louis, MO)	A7250
Protease Inhibitor Cocktail	Sigma-Aldrich (St.Louis, MO)	I3786
Phosphatase Inhibitor Cocktail	Sigma-Aldrich (St.Louis, MO)	P0044
Reference Dye for Quantitative PCR 100 ×, solution	Sigma-Aldrich (St.Louis, MO)	R4526
CELLBANKER 1	Takara (Shiga, Japan)	CB011
BCA Protein Assay Kit	Takara (Shiga, Japan)	T9300A
Trypsin-EDTA (0.05%)	Thermo Fisher Scientific (Waltham, MA)	25300062
Dead Cell Apoptosis Kit with Annexin V FITC and PI	Thermo Fisher Scientific (Waltham, MA)	V13242
CellEven Caspase-3/7 Green Flow Cytometry Assay Kit	Thermo Fisher Scientific (Waltham, MA)	C10427
FxCycle PI/RNase Staining Solution	Thermo Fisher Scientific (Waltham, MA)	F10797
RIPA Lysis and Extraction Buffer	Thermo Fisher Scientific (Waltham, MA)	89900
CellROX Orange Flow Cytometry Assay Kit	Thermo Fisher Scientific (Waltham, MA)	C10493
MitoSOX Red Mitochondrial Superoxide Indicator	Thermo Fisher Scientific (Waltham, MA)	M36008
Hanks' Balanced Salt solution	Thermo Fisher Scientific (Waltham, MA)	14025092
Power SYBR Green PCR Master Mix	Thermo Fisher Scientific (Waltham, MA)	4368706
Hoechst 33342	Thermo Fisher Scientific (Waltham, MA)	H3570
Lipofectamine RNAiMAX Transfection Reagent	Thermo Fisher Scientific (Waltham, MA)	13778030
CTS Opti-MEM I Medium	Thermo Fisher Scientific (Waltham, MA)	A4124801
Intracellular ATP assay kit ver.2	Toyo B-Net (Tokyo, Japan)	382-14581
Methanol	Wako (Osaka, Japan)	137-01823
Sodium Dodecyl Sulfate	Wako (Osaka, Japan)	194-13985

Supplementary Table 3. The top upregulated or downregulated gene sets based on NES >1.5 or <-1.5, and a normal *p*-value of <0.05 as the threshold. NES: normalized enrichment score; NOM, nominal; FDR: false discovery rate.

Hallmark

NAME	NES	NOM p-val	FDR q-val
HALLMARK_G2M_CHECKPOINT	-3.12	0.000	0.000
HALLMARK_E2F_TARGETS	-3.05	0.000	0.000
HALLMARK_MYC_TARGETS_V2	-2.87	0.000	0.000
HALLMARK_P53_PATHWAY	2.67	0.000	0.000
HALLMARK_MYC_TARGETS_V1	-2.62	0.000	0.000
HALLMARK_TNFA_SIGNALING_VIA_NFKB	2.40	0.000	0.000
HALLMARK_MITOTIC_SPINDLE	-2.36	0.000	0.000
HALLMARK_REACTIVE_OXYGEN_SPECIES_PATHWAY	2.23	0.000	0.000
HALLMARK_APOPTOSIS	2.16	0.000	0.000
HALLMARK_CHOLESTEROL_HOMEOSTASIS	2.15	0.000	0.000
HALLMARK_HEME_METABOLISM	2.02	0.000	0.000
HALLMARK_HYPOXIA	1.95	0.000	0.000
HALLMARK_XENOBIOTIC_METABOLISM	1.87	0.000	0.001
HALLMARK_INTERFERON_ALPHA_RESPONSE	-1.76	0.001	0.013
HALLMARK_UNFOLDED_PROTEIN_RESPONSE	-1.60	0.003	0.092
HALLMARK_BILE_ACID_METABOLISM	1.59	0.000	0.015
HALLMARK_SPERMATOGENESIS	-1.57	0.003	0.140

Gene Ontology

NAME	NES	NOM p-val	FDR q-val
GOCC_DNA_PACKAGING_COMPLEX	-3.08	0.000	0.000
GOBP_NUCLEOSOME_ASSEMBLY	-3.04	0.000	0.000
GOBP_NUCLEOSOME_ORGANIZATION	-2.93	0.000	0.000
GOBP_MITOTIC_SISTER_CHROMATID_SEGREGATION	-2.82	0.000	0.000
GOBP_DNA_CONFORMATION_CHANGE	-2.81	0.000	0.000

GOBP_DNA_REPLICATION_DEPENDENT_CHROMATIN_ORGANIZATION	-2.79	0.000	0.000
GOBP_PROTEIN_DNA_COMPLEX_ASSEMBLY	-2.79	0.000	0.000
GOCC_PROTEIN_DNA_COMPLEX	-2.79	0.000	0.000
GOBP_DNA_PACKAGING	-2.79	0.000	0.000
GOBP_PROTEIN_DNA_COMPLEX_SUBUNIT_ORGANIZATION	-2.77	0.000	0.000
GOBP_SISTER_CHROMATID_SEGREGATION	-2.76	0.000	0.000
GOCC_NUCLEAR_CHROMOSOME	-2.76	0.000	0.000
GOCC_CHROMOSOME_CENTROMERIC_REGION	-2.73	0.000	0.000
GOCC_PRERIBOSOME	-2.72	0.000	0.000
GOBP_CHROMATIN_ASSEMBLY_OR_DISASSEMBLY	-2.71	0.000	0.000
GOBP_RIBOSOME_BIOGENESIS	-2.69	0.000	0.000
GOBP_REGULATION_OF_CHROMOSOME_SEPARATION	-2.66	0.000	0.000
GOBP_MITOTIC_NUCLEAR_DIVISION	-2.66	0.000	0.000
GOBP_NUCLEAR_CHROMOSOME_SEGREGATION	-2.63	0.000	0.000
GOCC_CHROMOSOMAL_REGION	-2.62	0.000	0.000
GOBP_DNA_REPLICATION_INDEPENDENT_CHROMATIN_ORGANIZATION	-2.62	0.000	0.000
GOBP_REGULATION_OF_MITOTIC_SISTER_CHROMATID_SEGREGATION	-2.61	0.000	0.000
GOBP_CHROMOSOME_SEGREGATION	-2.61	0.000	0.000
GOBP_RRNA_METABOLIC_PROCESS	-2.59	0.000	0.000
GOBP_RIBONUCLEOPROTEIN_COMPLEX_BIOGENESIS	-2.59	0.000	0.000
GOBP_CHROMOSOME_SEPARATION	-2.58	0.000	0.000
GOBP_NEGATIVE_REGULATION_OF_MEGAKARYOCYTE_DIFFERENTIATION	-2.58	0.000	0.000
GOBP_CHROMATIN_REMODELING	-2.57	0.000	0.000
GOBP_NEGATIVE_REGULATION_OF_CHROMOSOME_ORGANIZATION	-2.54	0.000	0.000
GOBP_REGULATION_OF_CHROMOSOME_SEGREGATION	-2.53	0.000	0.000
GOBP_METAPHASE_ANAPHASE_TRANSITION_OF_CELL_CYCLE	-2.52	0.000	0.000
GOCC_CHROMOSOME_CENTROMERIC_CORE_DOMAIN	-2.50	0.000	0.000
GOBP_REGULATION_OF_CHROMOSOME_ORGANIZATION	-2.50	0.000	0.000
GOBP_NEGATIVE_REGULATION_OF_METAPHASE_ANAPHASE_TRANSITION_OF_CELL_CYCLE	-2.49	0.000	0.000
GOCC_CONDENSED_CHROMOSOME	-2.46	0.000	0.000
GOBP_NEGATIVE_REGULATION_OF_NUCLEAR_DIVISION	-2.46	0.000	0.000
GOBP_CHROMOSOME_CONDENSATION	-2.44	0.000	0.000
GOBP_MICROTUBULE_CYTOSKELETON_ORGANIZATION_INVOLVED_IN_MITOSIS	-2.44	0.000	0.000

GOCC_SECONDARY_LYSOSOME	2.44	0.000	0.001
GOBP_NCRNA_PROCESSING	-2.43	0.000	0.000
GOBP_RIBOSOMAL_SMALL_SUBUNIT_BIOGENESIS	-2.43	0.000	0.000
GOCC_CONDENSED_CHROMOSOME_CENTROMERIC_REGION	-2.42	0.000	0.000
GOBP_CHROMOSOME_LOCALIZATION	-2.38	0.000	0.000
GOBP_METAPHASE_PLATE_CONGRESSION	-2.38	0.000	0.000
GOBP_REGULATION_OF_MITOTIC_NUCLEAR_DIVISION	-2.37	0.000	0.000
GOBP_ORGANELLE_FISSION	-2.37	0.000	0.000
GOBP_DNA_DEPENDENT_DNA_REPLICATION	-2.36	0.000	0.000
GOBP_DNA_GEOMETRIC_CHANGE	-2.35	0.000	0.000
GOBP_TELOMERE_ORGANIZATION	-2.35	0.000	0.000
GOMF_SNORNA_BINDING	-2.35	0.000	0.000
GOBP_SPINDLE_ORGANIZATION	-2.35	0.000	0.000
GOCC_SPINDLE_POLE	-2.35	0.000	0.000
GOCC_90S_PRERIBOSOME	-2.34	0.000	0.000
GOBP_NCRNA_METABOLIC_PROCESS	-2.33	0.000	0.000
GOCC_PRERIBOSOME_LARGE_SUBUNIT_PRECURSOR	-2.33	0.000	0.000
GOBP_RIBOSOMAL_LARGE_SUBUNIT_BIOGENESIS	-2.33	0.000	0.000
GOMF_NUCLEOSOMAL_DNA_BINDING	-2.32	0.000	0.000
GOCC_AUTOPHAGOSOME	2.32	0.000	0.004
GOBP_RIBOSOME_ASSEMBLY	-2.32	0.000	0.000
GOMF_SINGLE_STRANDED_DNA_HELICASE_ACTIVITY	-2.31	0.000	0.000
GOBP_DNA_STRAND_ELONGATION	-2.30	0.000	0.000
GOBP_REGULATION_OF_NUCLEAR_DIVISION	-2.29	0.000	0.000
GOBP_MATURATION_OF_SSU_RRNA	-2.29	0.000	0.000
GOCC_CHROMOSOME_TELOMERIC_REGION	-2.28	0.000	0.000
GOBP_MITOTIC_SPINDLE_ORGANIZATION	-2.28	0.000	0.000
GOBP_CELLULAR_OXIDANT_DETOXIFICATION	2.28	0.000	0.006
GOMF_HELICASE_ACTIVITY	-2.27	0.000	0.000
GOBP_DNA_REPLICATION	-2.27	0.000	0.000
GOBP_CENTROMERE_COMPLEX_ASSEMBLY	-2.27	0.000	0.000
GOBP_MATURATION_OF_5_8S_RRNA	-2.27	0.000	0.000
GOMF_CATALYTIC_ACTIVITY_ACTING_ON_RNA	-2.26	0.000	0.000
GOBP_MATURATION_OF_SSU_RRNA_FROM_TRICISTRONIC_RRNA_TRANSCRI	-2.26	0.000	0.000
PT_SSU_RRNA_5_8S_RRNA_LSU_RRNA			

GOMF_PROTEIN_HETERODIMERIZATION_ACTIVITY	-2.26	0.000	0.000
GOBP_RNA_SPLICING_VIA_TRANSESTERIFICATION_REACTIONS	-2.25	0.000	0.000
GOCC_SPLICEOSOMAL_COMPLEX	-2.25	0.000	0.000
GOBP_PROTEIN_LOCALIZATION_TO_CHROMOSOME	-2.25	0.000	0.000
GOCC_SMALL_SUBUNIT_PROCESSOME	-2.25	0.000	0.000
GOCC_SPINDLE	-2.24	0.000	0.001
GOMF_ATP_DEPENDENT_ACTIVITY_ACTING_ON_DNA	-2.23	0.000	0.001
GOBP_ATTACHMENT_OF_SPINDLE_MICROTUBULES_TO_KINETOCHORE	-2.23	0.000	0.001
GOMF_DNA_HELICASE_ACTIVITY	-2.23	0.000	0.001
GOBP_REGULATION_OF_DNA_DEPENDENT_DNA_REPLICATION	-2.23	0.000	0.001
GOBP_SISTER_CHROMATID_COHESION	-2.23	0.000	0.001
GOBP_POSITIVE_REGULATION_OF_CELL_CYCLE_PROCESS	-2.23	0.000	0.002
GOBP_DNA_UNWINDING_INVOLVED_IN_DNA_REPLICATION	-2.22	0.000	0.002
GOBP_MITOTIC_METAPHASE_PLATE_CONGRESSION	-2.22	0.000	0.003
GOBP_NEGATIVE_REGULATION_OF_RNA_SPLICING	-2.22	0.000	0.003
GOMF_FERROUS_IRON_BINDING	2.22	0.000	0.011
GOMF_ANTIOXIDANT_ACTIVITY	2.21	0.000	0.009
GOMF_ATP_DEPENDENT_ACTIVITY_ACTING_ON_RNA	-2.21	0.000	0.003
GOBP_RIBOSOMAL_LARGE_SUBUNIT_ASSEMBLY	-2.21	0.000	0.003
GOBP_RNA_SPLICING	-2.21	0.000	0.003
GOBP_DNA_STRAND_ELONGATION_INVOLVED_IN_DNA_REPLICATION	-2.21	0.000	0.003
GOBP_PROTEIN_LOCALIZATION_TO_CHROMOSOME_CENTROMERIC_REGION	-2.20	0.000	0.004
GOBP_CLEAVAGE_INVOLVED_IN_RRNA_PROCESSING	-2.20	0.000	0.004
GOBP_REGULATION_OF_MEGAKARYOCYTE_DIFFERENTIATION	-2.20	0.000	0.004
GOBP_ESTABLISHMENT_OF_MITOTIC_SPINDLE_LOCALIZATION	-2.20	0.000	0.005
GOBP_MATURATION_OF_5_8S_RRNA_FROM_TRICISTRONIC_RRNA_TRANSCRI	-2.20	0.000	0.005
PT_SSU_RRNA_5_8S_RRNA_LSU_RRNA			
GOBP_PROSTANOID_BIOSYNTHETIC_PROCESS	2.19	0.000	0.012
GOBP_RESPONSE_TO_TYPE_I_INTERFERON	-2.19	0.000	0.006
GOMF_NUCLEOSOME_BINDING	-2.19	0.000	0.006
GOBP_PROTEIN_LOCALIZATION_TO_CONDENSED_CHROMOSOME	-2.18	0.000	0.006
GOBP_MEIOTIC_SPINDLE_ORGANIZATION	-2.18	0.000	0.006
GOCC_PRECATALYTIC_SPLICEOSOME	-2.18	0.000	0.006
GOCC_EXORIBONUCLEASE_COMPLEX	-2.17	0.000	0.008
GOCC_SPINDLE_MIDZONE	-2.17	0.000	0.009

GOBP_TRNA_METABOLIC_PROCESS	-2.16	0.000	0.011
GOCC_MITOTIC_SPINDLE	-2.15	0.000	0.011
GOBP_RNA_LOCALIZATION	-2.15	0.000	0.012
GOCC_SPLICEOSOMAL_TRI_SNRNP_COMPLEX	-2.15	0.000	0.012
GOBP_DNA_REPLICATION_INITIATION	-2.15	0.000	0.012
GOBP_RIBONUCLEOPROTEIN_COMPLEX_SUBUNIT_ORGANIZATION	-2.15	0.000	0.013
GOBP_NEGATIVE_REGULATION_OF_MRNA_SPLICING_VIA_SPLICEOSOME	-2.14	0.000	0.016
GOBP_MRNA_PROCESSING	-2.14	0.000	0.018
GOBP_SPINDLE_LOCALIZATION	-2.14	0.000	0.019
GOBP_NUCLEOSOME_POSITIONING	-2.14	0.000	0.020
GOCC_U2_TYPE_SPLICEOSOMAL_COMPLEX	-2.14	0.000	0.021
GOMF_ATP_HYDROLYSIS_ACTIVITY	-2.13	0.000	0.021
GOBP_RRNA_MODIFICATION	-2.13	0.000	0.021
GOBP_PROSTANOID_METABOLIC_PROCESS	2.13	0.000	0.025
GOBP_FEMALE_MEIOTIC_NUCLEAR_DIVISION	-2.12	0.000	0.024
GOBP_MITOTIC_CELL_CYCLE_PHASE_TRANSITION	-2.12	0.000	0.024
GOBP_BONE_RESORPTION	2.12	0.000	0.024
GOCC_PRERIBOSOME_SMALL_SUBUNIT_PRECURSOR	-2.12	0.000	0.024
GOBP_MACROAUTOPHAGY	2.12	0.000	0.022
GOBP_MEIOTIC_CHROMOSOME_SEGREGATION	-2.11	0.000	0.025
GOBP_MEGAKARYOCYTE_DIFFERENTIATION	-2.11	0.000	0.025
GOBP_SPINDLE_ASSEMBLY	-2.10	0.000	0.030
GOBP_KINETOCHORE_ORGANIZATION	-2.10	0.000	0.032
GOBP_REGULATION_OF_CELL_CYCLE_PHASE_TRANSITION	-2.10	0.000	0.036
GOBP_MRNA_EXPORT_FROM_NUCLEUS	-2.09	0.000	0.036
GOMF_CATALYTIC_ACTIVITY_ACTING_ON_A_TRNA	-2.09	0.000	0.037
GOBP_CELL_CYCLE_CHECKPOINT_SIGNALING	-2.09	0.000	0.038
GOBP_CELL_CYCLE_PHASE_TRANSITION	-2.09	0.000	0.038
GOBP_RESPONSE_TO_INTERFERON_BETA	-2.09	0.000	0.039
GOBP_MEIOTIC_CELL_CYCLE_PROCESS	-2.09	0.000	0.042
GOBP_REGULATION_OF_MITOTIC_CELL_CYCLE_PHASE_TRANSITION	-2.09	0.000	0.042
GOBP_AUTOPHAGOSOME_ORGANIZATION	2.08	0.000	0.033
GOCC_HETEROCHROMATIN	-2.08	0.000	0.049
GOBP_ESTABLISHMENT_OF_SPINDLE_ORIENTATION	-2.08	0.000	0.049
GOBP_GLUTATHIONE_METABOLIC_PROCESS	2.07	0.000	0.035

GOBP_DNA_REPAIR	-2.07	0.000	0.052
GOMF_CATALYTIC_ACTIVITY_ACTING_ON_DNA	-2.07	0.000	0.055
GOBP_CELLULAR_RESPONSE_TO_TOXIC_SUBSTANCE	2.06	0.000	0.035
GOBP_NON_MEMBRANE_BOUNDED_ORGANELLE_ASSEMBLY	-2.06	0.000	0.064
GOBP_DOUBLE_STRAND_BREAK_REPAIR	-2.06	0.000	0.066
GOBP_REGULATION_OF_DNA_REPLICATION	-2.06	0.000	0.066
GOCC_REPLICATION_FORK	-2.05	0.000	0.069
GOBP_MRNA_TRANSPORT	-2.05	0.000	0.072
GOCC_PHAGOPHORE_ASSEMBLY_SITE	2.05	0.000	0.042
GOBP_CELL_CYCLE_DNA_REPLICATION	-2.05	0.000	0.076
GOBP_REGULATION_OF_DNA_TEMPLATED_TRANSCRIPTION_IN_RESPONSE_TO_STRESS	2.04	0.000	0.042
GOBP_MITOTIC_SPINDLE_ASSEMBLY	-2.04	0.000	0.092
GOBP_RNA_PHOSPHODIESTER_BOND_HYDROLYSIS	-2.04	0.000	0.094
GOBP_MITOTIC_CHROMOSOME_CONDENSATION	-2.04	0.000	0.094
GOBP_DNA_RECOMBINATION	-2.03	0.000	0.118
GOBP_MEIOTIC_CELL_CYCLE	-2.03	0.000	0.120
GOBP_NEGATIVE_REGULATION_OF_MACROAUTOPHAGY	2.03	0.000	0.047
GOBP_NEGATIVE_REGULATION_OF_TYPE_I_INTERFERON_MEDIATED_SIGNALING_PATHWAY	-2.03	0.000	0.128
GOBP_RESPONSE_TO_AMINO_ACID_STARVATION	2.02	0.000	0.047
GOBP_RECOMBINATIONAL_REPAIR	-2.02	0.000	0.136
GOBP_NEGATIVE_REGULATION_OF_VIRAL_GENOME_REPLICATION	-2.02	0.000	0.139
GOBP_POSITIVE_REGULATION_OF_CELL_CYCLE_PHASE_TRANSITION	-2.02	0.000	0.150
GOBP_NEGATIVE_REGULATION_OF_CELL_CYCLE_PROCESS	-2.02	0.000	0.153
GOCC_SNO_S_RNA_CONTAINING_RIBONUCLEOPROTEIN_COMPLEX	-2.02	0.000	0.153
GOBP_REGULATION_OF_MITOTIC_CELL_CYCLE	-2.02	0.000	0.153
GOBP_POSITIVE_REGULATION_OF_CYTOKINESIS	-2.02	0.000	0.158
GOBP_ESTABLISHMENT_OF_RNA_LOCALIZATION	-2.01	0.000	0.167
GOBP_POSITIVE_REGULATION_OF_CELL_CYCLE	-2.01	0.000	0.173
GOBP_RNA_EXPORT_FROM_NUCLEUS	-2.01	0.000	0.183
GOBP_TRNA_PROCESSING	-2.01	0.000	0.185
GOBP_DETOXIFICATION	2.00	0.000	0.059
GOCC_CONDENSED_NUCLEAR_CHROMOSOME	-2.00	0.000	0.216

GOMF_EXONUCLEASE_ACTIVITY_ACTIVE_WITH_EITHER_RIBO_OR_DEOXYRIBONUCLEIC_ACIDS_AND_PRODUCING_5_PHOSPHOMONOESTERS	-1.99	0.000	0.220
GOCC_CATALYTIC_STEP_2_SPLICEOSOME	-1.99	0.000	0.226
GOBP_NEGATIVE_REGULATION_OF_MYELOID_CELL_DIFFERENTIATION	-1.99	0.000	0.229
GOCC_NUCLEOID	-1.99	0.000	0.235
GOBP_CHROMOSOME_ORGANIZATION_INVOLVED_IN_MEIOTIC_CELL_CYCLE	-1.98	0.000	0.249
GOBP_NUCLEOBASE_BIOSYNTHETIC_PROCESS	-1.98	0.000	0.250
GOMF_DNA_REPLICATION_ORIGIN_BINDING	-1.98	0.000	0.251
GOBP_NEGATIVE_REGULATION_OF_MRNA_PROCESSING	-1.98	0.000	0.254
GOBP_REGULATION_OF_MRNA_SPLICING_VIA_SPLICEOSOME	-1.98	0.000	0.255
GOBP_DNA_REPLICATION_CHECKPOINT_SIGNALING	-1.98	0.000	0.258
GOBP_NEGATIVE_REGULATION_OF_CELL_CYCLE_PHASE_TRANSITION	-1.98	0.000	0.258
GOBP_EMBRYONIC_SKELETAL_SYSTEM_MORPHOGENESIS	-1.98	0.000	0.261
GOBP_REGULATION_OF_MACROAUTOPHAGY	1.98	0.000	0.072
GOBP_ESTABLISHMENT_OF_PROTEIN_LOCALIZATION_TO_CHROMOSOME	-1.98	0.000	0.268
GOBP_TRANSLATIONAL_TERMINATION	-1.98	0.000	0.271
GOCC_SPINDLE_MICROTUBULE	-1.98	0.000	0.273
GOBP_POSITIVE_REGULATION_OF_RELEASE_OF_CYTOCHROME_C_FROM_MITOCHONDRIA	1.97	0.003	0.072
GOBP_REGULATION_OF_MICROGLIAL_CELL_ACTIVATION	1.97	0.000	0.069
GOBP_REGULATION_OF_RNA_SPLICING	-1.97	0.000	0.287
GOBP_RNA_METHYLATION	-1.97	0.000	0.290
GOBP_MITOTIC_CELL_CYCLE_CHECKPOINT_SIGNALING	-1.97	0.001	0.291
GOBP_KINETOCHORE_ASSEMBLY	-1.97	0.000	0.302
GOBP_AMYLOID_FIBRIL_FORMATION	1.97	0.000	0.068
GOBP_POSITIVE_REGULATION_OF_NEUROINFLAMMATORY_RESPONSE	1.97	0.003	0.065
GOCC_AUTOPHAGOSOME_MEMBRANE	1.97	0.000	0.063
GOBP_MATURATION_OF_LSU_RRNA	-1.97	0.000	0.315
GOBP_VIRAL_TRANSCRIPTION	-1.97	0.001	0.315
GOCC_CAJAL_BODY	-1.97	0.000	0.323
GOBP_REGULATION_OF_UBIQUITIN_PROTEIN_LIGASE_ACTIVITY	-1.96	0.000	0.336
GOBP_POSITIVE_REGULATION_OF_MACROAUTOPHAGY	1.96	0.000	0.065
GOBP_REGULATION_OF_TELOMERE_MAINTENANCE_VIA_TELOMERE_LENGTHENING	-1.96	0.001	0.363
GOMF_3_5_EXONUCLEASE_ACTIVITY	-1.96	0.000	0.364

GOBP_REGULATION_OF_CYTOKINESIS	-1.96	0.000	0.366
GOMF_STRUCTURAL_CONSTITUENT_OF_NUCLEAR_PORE	-1.95	0.000	0.379
GOBP_REGULATION_OF_TELOMERE_MAINTENANCE	-1.95	0.000	0.381
GOMF_3_5_DNA_HELICASE_ACTIVITY	-1.95	0.000	0.384
GOBP_REGULATION_OF_VACUOLE_ORGANIZATION	1.95	0.000	0.069
GOCC_DNA_POLYMERASE_COMPLEX	-1.95	0.000	0.386
GOBP_DNA_BIOSYNTHETIC_PROCESS	-1.95	0.000	0.386
GOMF_CATALYTIC_ACTIVITY_ACTING_ON_A_RRNA	-1.95	0.000	0.387
GOBP_NEURON_FATE_COMMITMENT	-1.95	0.000	0.387
GOMF_SINGLE_STRANDED_DNA_BINDING	-1.95	0.000	0.387
GOMF_EXONUCLEASE_ACTIVITY	-1.95	0.000	0.398
GOBP_POSITIVE_REGULATION_OF_CHROMOSOME_ORGANIZATION	-1.95	0.000	0.399
GOBP_RRNA_TRANSCRIPTION	-1.94	0.002	0.412
GOBP_REGULATION_OF_AUTOPHAGY	1.94	0.000	0.075
GOBP_RESPONSE_TO_INTERLEUKIN_4	-1.94	0.002	0.433
GOBP_NEGATIVE_REGULATION_OF_DNA_METABOLIC_PROCESS	-1.94	0.000	0.436
GOBP_NUCLEIC_ACID_PHOSPHODIESTER_BOND_HYDROLYSIS	-1.94	0.000	0.442
GOMF_RNA_METHYLTRANSFERASE_ACTIVITY	-1.93	0.000	0.459
GOBP_DNA_DEPENDENT_DNA_REPLICATION_MAINTENANCE_OF_FIDELITY	-1.93	0.000	0.459
GOBP_REGULATION_OF_BONE_RESORPTION	1.93	0.000	0.079
GOBP_RNA_MODIFICATION	-1.93	0.000	0.473
GOCC_MITOTIC_SPINDLE_POLE	-1.93	0.000	0.475
GOBP_REGULATION_OF_TYPE_I_INTERFERON_MEDIATED_SIGNALING_PATHWAY	-1.93	0.000	0.486
GOBP_NEGATIVE_REGULATION_OF_MITOTIC_CELL_CYCLE_PHASE_TRANSITION	-1.93	0.000	0.493
GOBP_REGULATION_OF_CELL_CYCLE_CHECKPOINT	-1.93	0.000	0.499
GOBP_TELOMERASE_RNA_LOCALIZATION	-1.93	0.000	0.505
GOBP_NUCLEOSOME_MOBILIZATION	-1.92	0.000	0.526
GOCC_MIDBODY	-1.92	0.000	0.527
GOBP_VACUOLAR_ACIDIFICATION	1.92	0.005	0.091
GOBP_REGULATION_OF_VIRAL_GENOME_REPLICATION	-1.91	0.001	0.580
GOMF_MRNA_5_UTR_BINDING	-1.91	0.000	0.580
GOBP_POSITIVE_REGULATION_OF_DNA_BIOSYNTHETIC_PROCESS	-1.91	0.000	0.580
GOBP_NEUTROPHIL_HOMEOSTASIS	1.91	0.000	0.091

GOBP_REGULATION_OF_MRNA_PROCESSING	-1.91	0.000	0.587
GOCC_LATE_ENDOSOME_MEMBRANE	1.91	0.000	0.089
GOBP_POSITIVE_REGULATION_OF_VACUOLE_ORGANIZATION	1.91	0.003	0.087
GOBP_RNA_PHOSPHODIESTER_BOND_HYDROLYSIS_ENDONUCLEOLYTIC	-1.91	0.000	0.605
GOBP_CYTOKINESIS	-1.91	0.000	0.631
GOBP_SELECTIVE_AUTOPHAGY	1.90	0.000	0.089
GOBP_NEGATIVE_REGULATION_OF_CELL_CYCLE	-1.90	0.000	0.641
GOBP_NCRNA_TRANSCRIPTION	-1.90	0.000	0.652
GOBP_PROTEIN_LOCALIZATION_TO_CHROMOSOME_TELOMERIC_REGION	-1.90	0.002	0.652
GOMF_GLUTATHIONE_PEROXIDASE_ACTIVITY	1.90	0.000	0.089
GOMF_EXORIBONUCLEASE_ACTIVITY	-1.90	0.000	0.662
GOMF_HISTONE_KINASE_ACTIVITY	-1.90	0.000	0.667
GOBP_REGULATION_OF_DNA_METABOLIC_PROCESS	-1.90	0.000	0.672
GOBP_RIBONUCLEOSIDE_MONOPHOSPHATE_BIOSYNTHETIC_PROCESS	-1.90	0.000	0.683
GOBP_INTRINSIC_APOPTOTIC_SIGNALING_PATHWAY_IN_RESPONSE_TO_DNA_DAMAGE_BY_P53_CLASS_MEDIATOR	1.90	0.000	0.092
GOBP_REGULATION_OF_DNA_BIOSYNTHETIC_PROCESS	-1.89	0.000	0.691
GOBP_RNA_5_END_PROCESSING	-1.89	0.002	0.696
GOBP_ATTACHMENT_OF_MITOTIC_SPINDLE_MICROTUBULES_TO_KINETOCORE	-1.89	0.002	0.702
GOBP_NEGATIVE_REGULATION_OF_VIRAL_PROCESS	-1.89	0.000	0.704
GOBP_RNA_PHOSPHODIESTER_BOND_HYDROLYSIS_EXONUCLEOLYTIC	-1.89	0.000	0.706
GOCC_ORGANELLAR_RIBOSOME	-1.89	0.000	0.713
GOBP_V_D_J_RECOMBINATION	-1.89	0.003	0.730
GOBP_NONRIBOSOMAL_PEPTIDE_BIOSYNTHETIC_PROCESS	1.89	0.003	0.099
GOBP_EMBRYONIC_SKELETAL_SYSTEM_DEVELOPMENT	-1.88	0.000	0.747
GOMF_NEUROPEPTIDE_RECEPTOR_BINDING	-1.88	0.000	0.752
GOCC_CHAPERONE_COMPLEX	-1.88	0.000	0.766
GOBP_TELOMERE_MAINTENANCE	-1.88	0.000	0.777
GOMF_PHOSPHATIDYLINOSITOL_3_4_BISPHOSPHATE_BINDING	1.88	0.006	0.103
GOCC_SPLICEOSOMAL_SNRNP_COMPLEX	-1.88	0.000	0.785
GOBP_REGULATION_OF_TRANSLATIONAL_FIDELITY	-1.88	0.000	0.785
GOBP_GLYCOSIDE_METABOLIC_PROCESS	1.88	0.000	0.102
GOBP_DNA_TEMPLATED_TRANSCRIPTION_INITIATION	-1.88	0.000	0.801
GOBP_POSITIVE_REGULATION_OF_MITOTIC_CELL_CYCLE	-1.87	0.000	0.808

GOBP_LYSOSOMAL_PROTEIN_CATABOLIC_PROCESS	1.87	0.000	0.103
GOMF_GLUTATHIONE_TRANSFERASE_ACTIVITY	1.87	0.000	0.101
GOBP_RRNA_METHYLATION	-1.87	0.000	0.825
GOBP_ICOSANOID_BIOSYNTHETIC_PROCESS	1.87	0.006	0.101
GOMF_TRNA_BINDING	-1.87	0.000	0.841
GOBP_NUCLEAR_TRANSCRIBED_MRNA_CATABOLIC_PROCESS_EXONUCLEOLYTIC	-1.86	0.003	0.855
GOBP_BONE_REMODELING	1.86	0.000	0.106
GOBP_ANAPHASE_PROMOTING_COMPLEX_DEPENDENT_CATABOLIC_PROCESS	-1.86	0.003	0.874
GOBP_NUCLEOSIDE_MONOPHOSPHATE_BIOSYNTHETIC_PROCESS	-1.86	0.000	0.875
GOCC_KINESIN_COMPLEX	-1.86	0.000	0.880
GOBP_SPLICEOSOMAL_SNRNP_ASSEMBLY	-1.86	0.000	0.881
GOBP_UNSATURATED_FATTY_ACID_BIOSYNTHETIC_PROCESS	1.86	0.000	0.109
GOBP_HOMOLOGOUS_CHROMOSOME_SEGREGATION	-1.85	0.001	0.893
GOBP_MITOTIC_CYTOKINESIS	-1.85	0.000	0.903
GOMF_PLUS_END_DIRECTED_MICROTUBULE_MOTOR_ACTIVITY	-1.85	0.000	0.909
GOCC_NUCLEAR_REPLICATION_FORK	-1.85	0.000	0.915
GOBP_TYPE_B_PANCREATIC_CELL_PROLIFERATION	1.85	0.003	0.117
GOBP_OSTEOCLAST_DIFFERENTIATION	1.85	0.000	0.115
GOBP_REGULATION_OF_GENE_EXPRESSION_EPIGENETIC	-1.85	0.000	0.917
GOBP_POSITIVE_REGULATION_OF_TELOMERE_MAINTENANCE	-1.84	0.000	0.923
GOBP_TRNA_MODIFICATION	-1.84	0.000	0.926
GOBP_MITOCHONDRIAL_GENE_EXPRESSION	-1.84	0.000	0.930
GOBP_REGULATION_OF_BONE_REMODELING	1.84	0.000	0.117
GOMF_FOUR_WAY_JUNCTION_DNA_BINDING	-1.84	0.003	0.930
GOBP_POSITIVE_REGULATION_OF_TELOMERE_MAINTENANCE_VIA_TELOMERE_LENGTHENING	-1.84	0.002	0.931
GOBP_CYTOSKELETON_DEPENDENT_CYTOKINESIS	-1.84	0.000	0.941
GOBP_INTRINSIC_APOPTOTIC_SIGNALING_PATHWAY_IN_RESPONSE_TO_DNA_DAMAGE	1.84	0.000	0.121
GOBP_POSITIVE_REGULATION_OF_MITOTIC_CELL_CYCLE_PHASE_TRANSITION	-1.84	0.001	0.942
GOBP_REGULATION_OF_DOUBLE_STRAND_BREAK_REPAIR	-1.83	0.000	0.955
GOBP_REGULATION_OF_NUCLEASE_ACTIVITY	-1.83	0.002	0.960

GOBP_PROTEIN_CATABOLIC_PROCESS_IN_THE_VACUOLE	1.83	0.003	0.126
GOBP_PURINE_NUCLEOSIDE_MONOPHOSPHATE_BIOSYNTHETIC_PROCESS	-1.83	0.000	0.961
GOBP_MRNA_MODIFICATION	-1.83	0.000	0.962
GOBP_MICROGLIAL_CELL_ACTIVATION	1.83	0.000	0.125
GOBP_NCRNA_CATABOLIC_PROCESS	-1.83	0.000	0.965
GOCC_SMN_SM_PROTEIN_COMPLEX	-1.83	0.002	0.965
GOBP_MITOCHONDRIAL_TRANSLATION	-1.83	0.000	0.965
GOBP_NEGATIVE_REGULATION_OF_DNA_RECOMBINATION	-1.82	0.003	0.967
GOBP_NCRNA_3_END_PROCESSING	-1.82	0.002	0.967
GOMF_RNA_POLYMERASE_ACTIVITY	-1.82	0.000	0.968
GOCC_ATPASE_COMPLEX	-1.82	0.000	0.972
GOBP_RESPONSE_TO_TOXIC_SUBSTANCE	1.82	0.000	0.133
GOBP_REGULATION_OF_MITOTIC_CELL_CYCLE_SPINDLE_ASSEMBLY_CHECK POINT	-1.82	0.003	0.975
GOMF_NUCLEASE_ACTIVITY	-1.82	0.000	0.975
GOBP_NUCLEOLAR_LARGE_RRNA_TRANSCRIPTION_BY_RNA_POLYMERASE_I	-1.82	0.007	0.975
GOBP_POSITIVE_REGULATION_OF_CELL_CYCLE_G1_S_PHASE_TRANSITION	-1.82	0.000	0.975
GOBP_RNA_DEPENDENT_DNA_BIOSYNTHETIC_PROCESS	-1.81	0.000	0.976
GOCC_GERM_CELL_NUCLEUS	-1.81	0.000	0.976
GOMF_EXORIBONUCLEASE_ACTIVITY_PRODUCING_5_PHOSPHOMONOESTER S	-1.81	0.000	0.978
GOBP_CELL_CYCLE_G2_M_PHASE_TRANSITION	-1.81	0.000	0.978
GOCC_SM_LIKE_PROTEIN_FAMILY_COMPLEX	-1.81	0.000	0.979
GOBP_DOUBLE_STRAND_BREAK_REPAIR_VIA_NONHOMOLOGOUS_END_JOINI NG	-1.81	0.000	0.980
GOMF_DNA_SECONDARY_STRUCTURE_BINDING	-1.81	0.000	0.983
GOBP_HISTONE_METHYLATION	-1.81	0.000	0.984
GOBP_CELL_REDOX_HOMEOSTASIS	1.80	0.000	0.149
GOBP_TRANSLATIONAL_INITIATION	-1.80	0.000	0.986
GOCC_RIBOSOME	-1.80	0.000	0.986
GOBP_POSITIVE_REGULATION_OF_TELOMERASE_RNA_LOCALIZATION_TO_C AJAL_BODY	-1.80	0.000	0.986
GOMF_LYSOPHOSPHOLIPASE_ACTIVITY	1.80	0.005	0.149
GOBP_RRNA_CATABOLIC_PROCESS	-1.80	0.003	0.990
GOBP_AMINO_ACID_ACTIVATION	-1.80	0.000	0.990

GOBP_POSITIVE_REGULATION_OF_BONE_RESORPTION	1.80	0.011	0.150
GOBP_UNSATURATED_FATTY_ACID_METABOLIC_PROCESS	1.80	0.000	0.151
GOBP_PLASMA_LIPOPROTEIN_PARTICLE_CLEARANCE	1.79	0.003	0.149
GOBP_PYRIMIDINE_NUCLEOTIDE_METABOLIC_PROCESS	-1.79	0.000	0.991
GOBP_REGULATION_OF_OSTEOCLAST_DIFFERENTIATION	1.79	0.000	0.148
GOCC_PHAGOPHORE_ASSEMBLY_SITE_MEMBRANE	1.79	0.008	0.148
GOBP_MEIOSIS_I_CELL_CYCLE_PROCESS	-1.79	0.000	0.991
GOCC_MITOCHONDRIAL_LARGE_RIBOSOMAL_SUBUNIT	-1.79	0.000	0.991
GOBP_NEGATIVE_REGULATION_OF_NUCLEOTIDE_METABOLIC_PROCESS	1.79	0.005	0.149
GOBP_ESTABLISHMENT_OF_PROTEIN_LOCALIZATION_TO_TELOMERE	-1.79	0.000	0.992
GOBP_NEGATIVE_REGULATION_OF_MITOTIC_CELL_CYCLE	-1.79	0.000	0.992
GOBP_PYRIMIDINE_DEOXYRIBONUCLEOTIDE_METABOLIC_PROCESS	-1.78	0.004	0.994
GOBP_EMBRYONIC_DIGESTIVE_TRACT_MORPHOGENESIS	-1.78	0.003	0.994
GOMF_METAL_CLUSTER_BINDING	-1.78	0.000	0.994
GOBP_NEGATIVE_REGULATION_OF_MRNA_METABOLIC_PROCESS	-1.78	0.001	0.995
GOBP_POSITIVE_REGULATION_OF_DNA_METABOLIC_PROCESS	-1.78	0.000	0.995
GOBP_CARDIAC_CONDUCTION_SYSTEM_DEVELOPMENT	-1.78	0.000	0.995
GOBP_AUTOPHAGY_OF_MITOCHONDRION	1.78	0.000	0.157
GOMF_4_IRON_4_SULFUR_CLUSTER_BINDING	-1.78	0.000	0.996
GOBP_NEGATIVE_REGULATION_OF_LIPASE_ACTIVITY	1.78	0.008	0.157
GOMF_S_ADENOSYLMETHIONINE_DEPENDENT_METHYLTRANSFERASE_ACTIVITY	-1.78	0.000	0.997
GOMF_DNA_BINDING_BENDING	-1.78	0.002	0.997
GOBP_NEURON_FATE_SPECIFICATION	-1.78	0.002	0.997
GOBP_INTRINSIC_APOPTOTIC_SIGNALING_PATHWAY_BY_P53_CLASS_MEDIATOR	1.78	0.000	0.158
GOCC_VACUOLAR_MEMBRANE	1.78	0.000	0.156
GOBP_INTERSTRAND_CROSS_LINK_REPAIR	-1.78	0.000	0.997
GOCC_METHYLTRANSFERASE_COMPLEX	-1.77	0.000	0.998
GOBP_POSITIVE_REGULATION_OF_TRANSCRIPTION_BY_RNA_POLYMERASE_I	-1.77	0.005	0.998
GOBP_ZINC_ION_HOMEOSTASIS	-1.77	0.001	0.998
GOMF_HISTONE_BINDING	-1.77	0.000	0.998
GOMF_TRANSFERASE_ACTIVITY_TRANSFERRING_ONE_CARBON_GROUPS	-1.77	0.000	0.998
GOBP_BROWN_FAT_CELL_DIFFERENTIATION	1.77	0.000	0.167

GOCC_LAMELLAR_BODY	1.77	0.010	0.165
GOCC_EARLY_ENDOSOME_MEMBRANE	1.77	0.000	0.163
GOBP_NUCLEOLUS_ORGANIZATION	-1.77	0.006	0.998
GOMF_DOUBLE_STRANDED_RNA_BINDING	-1.77	0.000	0.998
GOBP_TELOMERE_MAINTENANCE_VIA_TELOMERE_LENGTHENING	-1.77	0.000	0.998
GOBP_POSITIVE_REGULATION_OF_HISTONE_METHYLATION	-1.76	0.005	0.998
GOCC_U5_SNRNP	-1.76	0.002	0.998
GOBP_CENTRIOLE_ASSEMBLY	-1.76	0.003	0.998
GOCC_NUCLEAR_UBIQUITIN_LIGASE_COMPLEX	-1.76	0.001	0.998
GOMF_LIGASE_ACTIVITY_FORMING_CARBON_OXYGEN_BONDS	-1.76	0.001	0.998
GOCC_RIBOSOMAL_SUBUNIT	-1.76	0.000	0.998
GOBP_ICOSANOID_METABOLIC_PROCESS	1.76	0.000	0.169
GOBP_GROOMING_BEHAVIOR	-1.76	0.005	0.998
GOBP_NUCLEAR_EXPORT	-1.76	0.000	0.998
GOMF_SNRNA_BINDING	-1.76	0.004	0.998
GOBP_POSITIVE_REGULATION_OF_AUTOPHAGY	1.76	0.000	0.171
GOBP_REGULATION_OF_TRANSCRIPTION_BY_RNA_POLYMERASE_I	-1.76	0.002	0.998
GOBP_ANTIVIRAL_INNATE_IMMUNE_RESPONSE	-1.75	0.005	0.998
GOCC_ENDOSOME_MEMBRANE	1.75	0.000	0.173
GOBP_INTERMEDIATE_FILAMENT_BASED_PROCESS	1.75	0.003	0.172
GOBP_HISTONE_PHOSPHORYLATION	-1.75	0.003	0.998
GOBP_VACUOLE_ORGANIZATION	1.75	0.000	0.172
GOBP_POSITIVE_REGULATION_OF_RESPONSE_TO_DNA_DAMAGE_STIMULUS	-1.75	0.000	0.998
GOCC_AXONEMAL_DYNEIN_COMPLEX	1.75	0.006	0.174
GOBP_MICROTUBULE_NUCLEATION	-1.75	0.000	0.998
GOBP_REGULATION_OF_EXIT_FROM_MITOSIS	-1.75	0.005	0.998
GOBP_PROTEIN_TRANSMEMBRANE_TRANSPORT	-1.75	0.000	0.998
GOBP_RESPONSE_TO_ELECTRICAL_STIMULUS	1.74	0.000	0.177
GOBP_URETER_DEVELOPMENT	-1.74	0.008	0.998
GOCC_MRNA_CLEAVAGE_FACTOR_COMPLEX	-1.74	0.009	0.998
GOCC_GOLGI_CIS_CISTERNA	1.74	0.008	0.177
GOBP_REGULATION_OF_DNA_RECOMBINATION	-1.74	0.000	0.998
GOMF_PROTEIN_FOLDING_CHAPERONE	-1.74	0.005	0.998
GOBP_CELLULAR_IRON_ION_HOMEOSTASIS	1.74	0.000	0.177
GOMF_RRNA_BINDING	-1.74	0.000	0.998

GOCC_GLIAL_CELL_PROJECTION	1.74	0.011	0.176
GOBP_NUCLEUS_ORGANIZATION	-1.74	0.000	0.998
GOBP_REGULATION_OF_CELL_CYCLE_G2_M_PHASE_TRANSITION	-1.74	0.000	0.998
GOBP_POSITIVE_REGULATION_OF_DOUBLE_STRAND_BREAK_REPAIR	-1.74	0.000	0.998
GOMF_CHROMATIN_DNA_BINDING	-1.73	0.000	0.998
GOBP_NEURAL_CRESCENT_FORMATION	-1.73	0.008	0.998
GOBP_METHYLATION	-1.73	0.000	0.998
GOBP_PEPTIDYL_LYSINE_METHYLATION	-1.73	0.000	0.998
GOBP_AXONAL_TRANSPORT_OF_MITOCHONDRION	1.73	0.010	0.191
GOBP_POSITIVE_REGULATION_OF_DNA_REPAIR	-1.73	0.001	0.998
GOBP_CERAMIDE_CATABOLIC_PROCESS	1.73	0.016	0.189
GOBP_SKELETAL_MUSCLE_CELL_DIFFERENTIATION	1.73	0.003	0.189
GOBP_NEGATIVE_REGULATION_OF_HISTONE_MODIFICATION	-1.73	0.004	0.998
GOBP_REGULATION_OF_MRNA_METABOLIC_PROCESS	-1.72	0.000	0.998
GOMF_RIBONUCLEASE_ACTIVITY	-1.72	0.000	0.998
GOCC_FIBRILLAR_CENTER	-1.72	0.000	0.998
GOMF_DAMAGED_DNA_BINDING	-1.72	0.001	0.998
GOMF_NUCLEOTIDYLTRANSFERASE_ACTIVITY	-1.72	0.001	0.998
GOBP_VIRAL_GENOME_REPLICATION	-1.72	0.000	0.998
GOMF_OXIDOREDUCTASE_ACTIVITY_ACTING_ON_THE_CH_CH_GROUP_OF_D	1.72	0.018	0.196
ONORS_NAD_OR_NADP_AS_ACCEPTOR			
GOCC_ASTROCYTE_PROJECTION	1.72	0.007	0.196
GOBP_VASCULAR_WOUND_HEALING	-1.72	0.008	0.999
GOBP_DNA_TEMPLATED_TRANSCRIPTION_TERMINATION	-1.72	0.013	0.999
GOMF_ALCOHOL_DEHYDROGENASE_NADPPLUS_ACTIVITY	1.72	0.016	0.198
GOBP_SKELETAL_SYSTEM_MORPHOGENESIS	-1.71	0.000	0.999
GOBP_NEGATIVE_REGULATION_OF_DEVELOPMENTAL_GROWTH	1.71	0.000	0.197
GOMF_RIBONUCLEOPROTEIN_COMPLEX_BINDING	-1.71	0.000	0.999
GOBP_PEPTIDYL_LYSINE_TRIMETHYLATION	-1.71	0.004	0.999
GOCC_SYNAPTONEMAL_STRUCTURE	-1.71	0.006	0.999
GOBP_TRANSCRIPTION_BY_RNA_POLYMERASE_I	-1.71	0.001	0.999
GOBP_POSITIVE_REGULATION_OF_RHO_PROTEIN_SIGNAL_TRANSDUCTION	1.71	0.011	0.207
GOMF_MICROTUBULE_MOTOR_ACTIVITY	-1.71	0.003	1.000
GOBP_CENTROSOME_DUPLICATION	-1.71	0.001	1.000
GOBP_NEGATIVE_REGULATION_OF_HISTONE_METHYLATION	-1.70	0.013	1.000

GOBP_HISTONE_MODIFICATION	-1.70	0.000	1.000
GOCC_LARGE_RIBOSOMAL_SUBUNIT	-1.70	0.000	1.000
GOBP_EMBRYONIC_ORGAN_MORPHOGENESIS	-1.70	0.000	1.000
GOBP_REGULATION_OF_HISTONE_METHYLATION	-1.70	0.000	1.000
GOBP_MICROTUBULE_BASED_TRANSPORT	1.70	0.000	0.214
GOCC_EUCHROMATIN	-1.70	0.002	1.000
GOBP_SNRNA_PROCESSING	-1.70	0.011	1.000
GOCC_CELL_DIVISION_SITE	-1.70	0.003	1.000
GOBP_AUTOPHAGOSOME_MATURATION	1.70	0.003	0.215
GOBP_REGULATION_OF_DNA_METHYLATION	-1.70	0.007	1.000
GOBP_NUCLEOSIDE_MONOPHOSPHATE_METABOLIC_PROCESS	-1.70	0.000	1.000
GOBP_MITOTIC_SISTER_CHROMATID_COHESION	-1.69	0.011	1.000
GOBP_CELLULAR_RESPONSE_TO_CHEMICAL_STRESS	1.69	0.000	0.220
GOBP_POSITIVE_REGULATION_OF_NATURAL_KILLER_CELL_ACTIVATION	1.69	0.009	0.220
GOMF_MAGNESIUM_ION_TRANSMEMBRANE_TRANSPORTER_ACTIVITY	1.69	0.018	0.217
GOBP_NEGATIVE_REGULATION_OF_NIK_NF_KAPPAB_SIGNALING	1.69	0.020	0.215
GOBP_REGULATION_OF_CELL_DIVISION	-1.69	0.000	1.000
GOBP_POSITIVE_REGULATION_OF_HISTONE_MODIFICATION	-1.69	0.000	1.000
GOCC_ANAPHASE_PROMOTING_COMPLEX	-1.69	0.014	1.000
GOBP_RNA_3_END_PROCESSING	-1.69	0.000	1.000
GOBP_CELLULAR_RESPONSE_TO_ZINC_ION	-1.69	0.011	1.000
GOCC_LATE_ENDOSOME	1.69	0.000	0.222
GOBP_NEGATIVE_REGULATION_OF_STRIATED_MUSCLE_CELL_APOPTOTIC_PROCESS	1.69	0.006	0.220
GOMF_HORMONE_RECEPTOR_BINDING	-1.69	0.011	1.000
GOBP_REGULATION_OF_EPITHELIAL_CELL_APOPTOTIC_PROCESS	1.69	0.004	0.219
GOBP_MICROTUBULE_ORGANIZING_CENTER_ORGANIZATION	-1.69	0.001	1.000
GOBP_MAGNESIUM_ION_TRANSPORT	1.69	0.016	0.217
GOBP_ANGIOGENESIS_INVOLVED_IN_WOUND_HEALING	-1.69	0.013	1.000
GOBP_BASE_EXCISION_REPAIR	-1.68	0.002	1.000
GOBP_RESPONSE_TO_ISCHEMIA	1.68	0.000	0.219
GOMF_MRNA_BINDING	-1.68	0.000	1.000
GOBP_DNA_INTEGRITY_CHECKPOINT_SIGNALING	-1.68	0.000	1.000
GOBP_STEROL_BIOSYNTHETIC_PROCESS	1.68	0.000	0.218
GOMF_TELOMERIC_DNA_BINDING	-1.68	0.006	1.000

GOMF_RETINAL_BINDING	-1.68	0.006	1.000
GOMF_CALMODULIN_DEPENDENT_PROTEIN_KINASE_ACTIVITY	-1.68	0.008	1.000
GOBP_REGULATION_OF_TRANSCRIPTION_OF_NUCLEOLAR_LARGE_RRNA_BY_RNA_POLYMERASE_I	-1.68	0.008	1.000
GOBP_NEUROINFLAMMATORY_RESPONSE	1.68	0.012	0.219
GOCC_MRNA_CLEAVAGE_AND_POLYADENYLATION_SPECIFICITY_FACTOR_COMPLEX	-1.68	0.009	1.000
GOCC_U12_TYPE_SPLICEOSOMAL_COMPLEX	-1.68	0.008	1.000
GOBP_TRNA_METHYLATION	-1.68	0.003	1.000
GOCC_DNA_REPAIR_COMPLEX	-1.68	0.006	1.000
GOBP_G1_TO_G0_TRANSITION	-1.68	0.013	1.000
GOBP_LEFT_RIGHT_PATTERN_FORMATION	1.68	0.015	0.225
GOBP_MITOCHONDRIAL_RNA_METABOLIC_PROCESS	-1.68	0.001	1.000
GOBP_POSITIVE_REGULATION_OF_CELL_CYCLE_G2_M_PHASE_TRANSITION	-1.67	0.008	1.000
GOBP_NEGATIVE_REGULATION_OF_VIRAL_LIFE_CYCLE	-1.67	0.008	1.000
GOBP_MITOCHONDRIAL_TRANSMEMBRANE_TRANSPORT	-1.67	0.006	1.000
GOBP_REGULATION_OF_SISTER_CHROMATID_COHESION	-1.67	0.010	1.000
GOBP_PSEUDOURIDINE_SYNTHESIS	-1.67	0.006	1.000
GOBP_MEIOTIC_CHROMOSOME_SEPARATION	-1.67	0.011	1.000
GOMF_TRNA_METHYLTRANSFERASE_ACTIVITY	-1.67	0.005	1.000
GOBP_NUCLEOBASE_CONTAINING_COMPOUND_TRANSPORT	-1.67	0.000	1.000
GOBP_REGULATION_OF_DNA_REPAIR	-1.67	0.001	1.000
GOBP_PROTEIN_LOCALIZATION_TO_CHROMATIN	-1.67	0.003	1.000
GOBP_NEGATIVE_REGULATION_OF_HISTONE_ACETYLATION	-1.67	0.014	1.000
GOMF_UNFOLDED_PROTEIN_BINDING	-1.67	0.000	1.000
GOBP_POSITIVE_REGULATION_OF_MRNA_SPLICING_VIA_SPLICEOSOME	-1.67	0.006	1.000
GOBP_CEREBELLAR_PURKINJE_CELL_LAYER_DEVELOPMENT	-1.67	0.006	1.000
GOCC_RESPIRATORY_CHAIN_COMPLEX_IV	1.67	0.031	0.239
GOBP_REPLICATION_FORK_PROCESSING	-1.67	0.004	1.000
GOBP_ANTERIOR_POSTERIOR_PATTERN_SPECIFICATION	-1.67	0.000	1.000
GOBP_REGULATION_OF_CYCLIN_DEPENDENT_PROTEIN_KINASE_ACTIVITY	-1.66	0.000	1.000
GOBP_AXO_DENDRITIC_TRANSPORT	1.66	0.008	0.243
GOCC_REPLISOME	-1.66	0.008	1.000
GOCC_CIS_GOLGI_NETWORK	1.66	0.003	0.241
GOBP_CELLULAR_RESPONSE_TO_PROSTAGLANDIN_STIMULUS	1.66	0.021	0.239

GOMF_PROTEIN_KINASE_C_BINDING	1.66	0.000	0.237
GOBP_REGULATION_OF_PHOSPHATIDYLINOSITOL_3_KINASE_ACTIVITY	-1.66	0.009	1.000
GOBP_PIGMENT_GRANULE_ORGANIZATION	1.66	0.016	0.235
GOBP_CELL_CYCLE_G1_S_PHASE_TRANSITION	-1.66	0.001	1.000
GOBP_RESPONSE_TO_OXYGEN_RADICAL	1.66	0.029	0.236
GOBP_REGULATION_OF_HISTONE_MODIFICATION	-1.66	0.000	1.000
GOBP_POSITIVE_REGULATION_OF_MITOTIC_NUCLEAR_DIVISION	-1.66	0.005	1.000
GOBP_MRNA_CLEAVAGE	-1.66	0.019	1.000
GOBP_MEMBRANE_LIPID_CATABOLIC_PROCESS	1.65	0.015	0.244
GOBP_REGULATION_OF_MEIOTIC_CELL_CYCLE	-1.65	0.003	1.000
GOBP_RNA_CATABOLIC_PROCESS	-1.65	0.000	1.000
GOMF_ENDORIBONUCLEASE_ACTIVITY_PRODUCING_5_PHOSPHOMONOESTERS	-1.65	0.011	1.000
GOBP_AMP_METABOLIC_PROCESS	-1.65	0.012	1.000
GOBP_EMBRYONIC_ORGAN_DEVELOPMENT	-1.65	0.000	1.000
GOBP_EPITHELIAL_TUBE_BRANCHING_INVOLVED_IN_LUNG_MORPHOGENESIS	-1.65	0.014	1.000
GOMF_STRUCTURAL_CONSTITUENT_OF_RIBOSOME	-1.65	0.001	1.000
GOBP_ALTERNATIVE_MRNA_SPLICING_VIA_SPLICEOSOME	-1.65	0.004	1.000
GOMF_PROTEIN_SERINE_THREONINE_KINASE_ACTIVATOR_ACTIVITY	-1.65	0.006	1.000
GOBP_REGULATION_OF_SPINDLE_ORGANIZATION	-1.65	0.013	1.000
GOBP_CHEMOKINE_PRODUCTION	1.65	0.004	0.255
GOBP_CALCIIUM_DEPENDENT_CELL_CELL_ADHESION_VIA_PLASMA_MEMBRANE_CELL_ADHESION_MOLECULES	1.65	0.008	0.255
GOMF_N_METHYLTRANSFERASE_ACTIVITY	-1.65	0.001	1.000
GOBP_INTRACELLULAR_PROTEIN_TRANSMEMBRANE_TRANSPORT	-1.64	0.001	1.000
GOBP_REGULATION_OF_SUPEROXIDE_METABOLIC_PROCESS	1.64	0.012	0.257
GOBP_TRANSPORT_ALONG_MICROTUBULE	1.64	0.000	0.256
GOBP_OLIGOSACCHARIDE_LIPID_INTERMEDIATE_BIOSYNTHETIC_PROCESS	-1.64	0.016	1.000
GOBP_VIRAL_GENE_EXPRESSION	-1.64	0.000	1.000
GOMF_P53_BINDING	-1.64	0.009	1.000
GOBP_POSITIVE_REGULATION_OF_ATP_DEPENDENT_ACTIVITY	-1.64	0.006	1.000
GOBP_POSITIVE_REGULATION_OF_TRANSCRIPTION_FROM_RNA_POLYMERASE_II_PROMOTER_IN_RESPONSE_TO_STRESS	1.64	0.014	0.256
GOBP_PROTEIN_DNA_COMPLEX_DISASSEMBLY	-1.64	0.018	1.000

GOCC_APICAL_DENDRITE	1.64	0.025	0.258
GOMF_RETINOL_BINDING	-1.64	0.010	1.000
GOBP_NEGATIVE_REGULATION_OF_PEPTIDYL_LYSINE_ACETYLATION	-1.64	0.011	1.000
GOBP_NEGATIVE_REGULATION_OF_AXON_EXTENSION	1.64	0.009	0.260
GOCC_RNA_POLYMERASE_COMPLEX	-1.64	0.000	1.000
GOBP_INNATE_IMMUNE_RESPONSE_IN_MUCOSA	-1.64	0.018	1.000
GOCC_TRICARBOXYLIC_ACID_CYCLE_ENZYME_COMPLEX	-1.64	0.007	1.000
GOBP_QUINONE_METABOLIC_PROCESS	1.63	0.015	0.263
GOCC_SITE_OF_DNA_DAMAGE	-1.63	0.003	1.000
GOBP_LATE_ENDOSOME_TO_LYSOSOME_TRANSPORT	1.63	0.029	0.263
GOBP_NEGATIVE_REGULATION_OF_MACROPHAGE_ACTIVATION	1.63	0.019	0.261
GOBP_ANATOMICAL_STRUCTURE_REGRESSION	-1.63	0.020	1.000
GOBP_REGULATION_OF_HISTONE_H3_K9_METHYLATION	-1.63	0.017	1.000
GOCC_VOLTAGE_GATED_SODIUM_CHANNEL_COMPLEX	1.63	0.018	0.263
GOBP_INTRINSIC_APOPTOTIC_SIGNALING_PATHWAY	1.63	0.000	0.261
GOBP_PYRIMIDINE_NUCLEOTIDE_CATABOLIC_PROCESS	-1.63	0.017	1.000
GOBP_REGULATION_OF_TRANSCRIPTION_REGULATORY_REGION_DNA_BINDING	-1.63	0.003	1.000
GOMF_NEUROPEPTIDE_HORMONE_ACTIVITY	-1.63	0.018	1.000
GOBP_SNRNA_METABOLIC_PROCESS	-1.63	0.002	1.000
GOBP_HISTONE_H3_K27_METHYLATION	-1.63	0.010	1.000
GOBP_NEGATIVE_REGULATION_OF_PROTEIN_ACETYLATION	-1.63	0.018	1.000
GOBP_OLIGODENDROCYTE_DIFFERENTIATION	-1.63	0.001	1.000
GOBP_IMMUNOLOGICAL_MEMORY_PROCESS	1.63	0.019	0.266
GOBP_MHC_CLASS_II_BIOSYNTHETIC_PROCESS	-1.63	0.017	1.000
GOBP_NEGATIVE_REGULATION_OF_SMALL_MOLECULE_METABOLIC_PROCESSES	1.63	0.007	0.265
GOBP_ESTABLISHMENT_OF_PIGMENT_GRANULE_LOCALIZATION	1.63	0.032	0.263
GOBP_DNA_DAMAGE_RESPONSE_SIGNAL_TRANSDUCTION_BY_P53_CLASS_MEDIATOR_RESULTING_IN_CELL_CYCLE_ARREST	1.63	0.028	0.262
GOBP_NEGATIVE_REGULATION_OF_NEURAL_PRECURSOR_CELL_PROLIFERATION	1.63	0.034	0.260
GOBP_PROTEIN_FOLDING	-1.62	0.000	1.000
GOBP_FAT_CELL_DIFFERENTIATION	1.62	0.000	0.260
GOBP_POSITIVE_REGULATION_OF_CHEMOKINE_PRODUCTION	1.62	0.000	0.258

GOBP_HISTONE_MRNA_METABOLIC_PROCESS	-1.62	0.015	1.000
GOBP_HINDLIMB_MORPHOGENESIS	-1.62	0.009	1.000
GOBP_PH_REDUCTION	1.62	0.019	0.258
GOCC_MALE_GERM_CELL_NUCLEUS	-1.62	0.023	1.000
GOBP_PROTEIN_METHYLATION	-1.62	0.000	1.000
GOBP_COLLECTING_DUCT_DEVELOPMENT	1.62	0.033	0.257
GOMF_TRANSLATION_FACTOR_ACTIVITY_RNA_BINDING	-1.62	0.004	1.000
GOBP_REGULATION_OF_VIRAL_PROCESS	-1.62	0.001	1.000
GOBP_POSITIVE_REGULATION_OF_DOUBLE_STRAND_BREAK_REPAIR_VIA_N ONHOMOLOGOUS_END_JOINING	-1.62	0.016	1.000
GOMF_GLYCOSYLTRANSFERASE_ACTIVITY	-1.62	0.024	1.000
GOBP_PYRIMIDINE_NUCLEOSIDE_TRIPHOSPHATE_METABOLIC_PROCESS	-1.62	0.016	1.000
GOBP_EMBRYONIC_DIGESTIVE_TRACT_DEVELOPMENT	-1.62	0.013	1.000
GOBP_STEROID_BIOSYNTHETIC_PROCESS	1.62	0.000	0.261
GOBP_SOMATIC_DIVERSIFICATION_OF_IMMUNE_RECEPTORS	-1.62	0.003	1.000
GOBP_REGULATION_OF_CHROMATIN_BINDING	-1.62	0.018	1.000
GOBP_CELLULAR_RESPONSE_TO_EXTERNAL_STIMULUS	1.62	0.000	0.262
GOBP_EXIT_FROM_MITOSIS	-1.62	0.014	1.000
GOBP_PROTEIN_TRANSMEMBRANE_IMPORT_INTO_INTRACELLULAR_ORGAN ELLE	-1.62	0.009	1.000
GOBP_NUCLEAR_TRANSPORT	-1.62	0.000	1.000
GOBP_LYSOSOMAL_TRANSPORT	1.61	0.004	0.266
GOBP_RIBONUCLEOSIDE_MONOPHOSPHATE_METABOLIC_PROCESS	-1.61	0.003	1.000
GOBP_REGULATION_OF_DOUBLE_STRAND_BREAK_REPAIR_VIA_NONHOMOL OGOUS_END_JOINING	-1.61	0.016	1.000
GOBP_LACTATION	-1.61	0.019	1.000
GOCC_MITOCHONDRIAL_MATRIX	-1.61	0.000	1.000
GOBP_NEGATIVE_REGULATION_OF_STRIATED_MUSCLE_CELL_DIFFERENTIAT ION	-1.61	0.009	1.000
GOBP_NEGATIVE_REGULATION_OF_TELOMERE_MAINTENANCE	-1.61	0.011	1.000
GOBP_MITOCHONDRIAL_RNA_PROCESSING	-1.61	0.018	1.000
GOCC_NUCLEAR_SPECK	-1.61	0.000	1.000
GOBP_PHOSPHATE_ION_TRANSMEMBRANE_TRANSPORT	-1.61	0.028	1.000
GOMF_PHOSPHATIDYLINOSITOL_3_KINASE_REGULATOR_ACTIVITY	-1.61	0.015	1.000
GOMF_TELOMERASE_RNA_BINDING	-1.61	0.027	1.000

GOBP_EMBRYONIC_EYE_MORPHOGENESIS	-1.61	0.014	1.000
GOBP_SPLICEOSOMAL_COMPLEX_ASSEMBLY	-1.61	0.007	1.000
GOBP_REGULATION_OF_GLIAL_CELL_MIGRATION	1.61	0.037	0.279
GOBP_NUCLEOBASE_METABOLIC_PROCESS	-1.61	0.007	1.000
GOMF_LONG_CHAIN_FATTY_ACID_TRANSPORTER_ACTIVITY	-1.61	0.021	1.000
GOCC_NUCLEAR_PORE	-1.61	0.003	1.000
GOMF_ENDONUCLEASE_ACTIVITY_ACTIVE_WITH_EITHER_RIBO_OR_DEOXYRI BONUCLEIC_ACIDS_AND_PRODUCING_5_PHOSPHOMONOESTERS	-1.61	0.013	1.000
GOMF_BHLH_TRANSCRIPTION_FACTOR_BINDING	-1.61	0.017	1.000
GOBP_IMP_METABOLIC_PROCESS	-1.61	0.023	1.000
GOBP_AXONAL_TRANSPORT	1.60	0.006	0.282
GOCC_CENTRIOLE	-1.60	0.001	1.000
GOCC_U2_TYPE_CATALYTIC_STEP_2_SPLICEOSOME	-1.60	0.014	1.000
GOBP_IRON_ION_TRANSPORT	1.60	0.009	0.281
GOBP_CELLULAR_RESPONSE_TO_STARVATION	1.60	0.000	0.281
GOBP_RESPONSE_TO_COCAINE	-1.60	0.016	1.000
GOCC_CLEAVAGE_FURROW	-1.60	0.012	1.000
GOBP_MICROTUBULE_POLYMERIZATION_OR_DEPOLYMERIZATION	-1.60	0.003	1.000
GOBP_NEGATIVE_REGULATION_OF_INTRINSIC_APOPTOTIC_SIGNALING_PAT HWAY_IN_RESPONSE_TO_DNA_DAMAGE	1.60	0.020	0.281
GOCC_U2_SNRNP	-1.60	0.024	1.000
GOCC_PERICENTRIC_HETEROCHROMATIN	-1.60	0.023	1.000
GOBP_POSITIVE_REGULATION_OF_RNA_SPLICING	-1.60	0.015	1.000
GOBP_INTERLEUKIN_6_MEDIATED_SIGNALING_PATHWAY	1.60	0.039	0.281
GOBP_TRNA_5_END_PROCESSING	-1.60	0.015	1.000
GOMF_SULFUR_COMPOUND_TRANSMEMBRANE_TRANSPORTER_ACTIVITY	1.60	0.006	0.280
GOBP_EMBRYONIC_APPENDAGE_MORPHOGENESIS	-1.60	0.003	1.000
GOBP_BLASTOCYST_GROWTH	-1.60	0.013	1.000
GOCC_ENDORIBONUCLEASE_COMPLEX	-1.60	0.014	1.000
GOBP_POSITIVE_REGULATION_OF_TRANSLATIONAL_INITIATION	-1.60	0.014	1.000
GOBP_IRON_ION_HOMEOSTASIS	1.60	0.003	0.284
GOBP_INTERLEUKIN_5_PRODUCTION	-1.60	0.029	1.000
GOCC_PRESPLICEOSOME	-1.60	0.027	1.000
GOBP_CELLULAR_RESPONSE_TO_REACTIVE_NITROGEN_SPECIES	-1.59	0.013	1.000
GOBP_TISSUE_REMODELING	1.59	0.000	0.287

GOBP_EPIDERMIS_MORPHOGENESIS	1.59	0.030	0.288
GOBP_NUCLEAR_TRANSCRIBED_MRNA_CATABOLIC_PROCESS_NONSENSE_MEDIATED_DECAY	-1.59	0.006	1.000
GOBP_PROGESTERONE_METABOLIC_PROCESS	1.59	0.044	0.288
GOBP_RESPONSE_TO_ACID_CHEMICAL	1.59	0.004	0.286
GOBP_ARACHIDONIC_ACID_METABOLIC_PROCESS	1.59	0.009	0.285
GOBP_NEGATIVE_REGULATION_OF_NEURON_DEATH	1.59	0.000	0.285
GOBP_POSITIVE_REGULATION_OF_TYPE_I_INTERFERON_PRODUCTION	-1.59	0.006	1.000
GOBP_RIBOSOMAL_SMALL_SUBUNIT_ASSEMBLY	-1.59	0.016	1.000
GOCC_PROTEIN_COMPLEX_INVOLVED_IN_CELL_ADHESION	-1.59	0.015	1.000
GOBP_MEMORY	1.59	0.000	0.288
GOCC_MITOCHONDRIAL_PROTEIN_CONTAINING_COMPLEX	-1.59	0.001	1.000
GOCC_STEREOCILUM_BUNDLE	1.59	0.003	0.290
GOBP_REGULATION_OF_DOUBLE_STRAND_BREAK_REPAIR_VIA_HOMOLOGOUS_RECOMBINATION	-1.59	0.006	1.000
GOBP_NEGATIVE_REGULATION_OF_UBIQUITIN_PROTEIN_TRANSFERASE_ACTIVITY	-1.59	0.014	1.000
GOBP_GLYCOPROTEIN_CATABOLIC_PROCESS	1.58	0.026	0.289
GOBP_RESPONSE_TO_FOLLICLE_STIMULATING_HORMONE	1.58	0.049	0.288
GOBP_POSITIVE_REGULATION_OF_VIRAL_GENOME_REPLICATION	-1.58	0.011	1.000
GOBP_RESPONSE_TO_STARVATION	1.58	0.000	0.287
GOMF_CARBOHYDRATE_CATION_SYMPORTER_ACTIVITY	1.58	0.041	0.288
GOMF_BILE_ACID_TRANSMEMBRANE_TRANSPORTER_ACTIVITY	1.58	0.050	0.287
GOBP_VACUOLAR_TRANSPORT	1.58	0.004	0.285
GOMF_DNA_POLYMERASE_BINDING	-1.58	0.027	1.000
GOBP_SPERM_FLAGELLUM_ASSEMBLY	1.58	0.018	0.285
GOBP_DNA_SYNTHESIS_INVOLVED_IN_DNA_REPAIR	-1.58	0.014	1.000
GOBP_REGULATION_OF_LIPID_KINASE_ACTIVITY	-1.58	0.015	1.000
GOBP_NEGATIVE_REGULATION_OF_GENE_EXPRESSION_EPIGENETIC	-1.58	0.006	1.000
GOBP_NEGATIVE_REGULATION_OF_CYTOKINE_PRODUCTION_INVOLVED_IN_IMMUNE_INFLAMMATORY_RESPONSE	1.58	0.033	0.285
GOBP_APPENDAGE_MORPHOGENESIS	-1.58	0.003	1.000
GOBP_NEGATIVE_REGULATION_OF_AXONOGENESIS	1.58	0.013	0.288
GOMF_METHYL_CPG_BINDING	-1.58	0.016	1.000
GOBP_REGULATION_OF_OLIGODENDROCYTE_DIFFERENTIATION	-1.57	0.010	1.000

GOCC_INTRINSIC_COMPONENT_OF_NUCLEAR_INNER_MEMBRANE	-1.57	0.021	1.000
GOBP_EMBRYONIC_HINDLIMB_MORPHOGENESIS	-1.57	0.030	1.000
GOBP_MAINTENANCE_OF_CELL_NUMBER	-1.57	0.003	1.000
GOBP_RESPONSE_TO_OXIDATIVE_STRESS	1.57	0.000	0.295
GOBP_CELLULAR_RESPONSE_TO_CADMIUM_ION	1.57	0.017	0.293
GOBP_REGULATION_OF_CENTRIOLE_REPLICATION	-1.57	0.023	1.000
GOBP_HEAT_GENERATION	1.57	0.045	0.297
GOMF_POLY_PYRIMIDINE_TRACT_BINDING	-1.57	0.017	1.000
GOBP_SUPEROXIDE_METABOLIC_PROCESS	1.57	0.016	0.295
GOBP_PROTEIN_LOCALIZATION_TO_NUCLEUS	-1.57	0.001	1.000
GOBP_RESPONSE_TO_ARSENIC_CONTAINING_SUBSTANCE	1.57	0.025	0.298
GOBP_CELLULAR_RESPONSE_TO_MECHANICAL_STIMULUS	1.57	0.012	0.298
GOMF_HISTONE_METHYLTRANSFERASE_ACTIVITY	-1.57	0.020	1.000
GOBP_BLASTOCYST_DEVELOPMENT	-1.57	0.004	1.000
GOBP_RAB_PROTEIN_SIGNAL_TRANSDUCTION	1.57	0.030	0.298
GOBP_HISTONE_H3_K4_METHYLATION	-1.57	0.010	1.000
GOBP_TORC1_SIGNALING	1.56	0.018	0.297
GOBP_POSITIVE_REGULATION_OF_TELOMERE_CAPPING	-1.56	0.045	1.000
GOMF_RETINOIC_ACID_BINDING	-1.56	0.031	1.000
GOCC_PROTEASOME_ACCESSORY_COMPLEX	-1.56	0.027	1.000
GOMF_VITAMIN_TRANSMEMBRANE_TRANSPORTER_ACTIVITY	-1.56	0.020	1.000
GOBP_ROOF_OF_MOUTH_DEVELOPMENT	-1.56	0.007	1.000
GOBP_RESPONSE_TO_REACTIVE_OXYGEN_SPECIES	1.56	0.000	0.297
GOCC_ORGANELLE_ENVELOPE_LUMEN	-1.56	0.007	1.000
GOMF_HYDROLASE_ACTIVITY_ACTING_ON_CARBON_NITROGEN_BUT_NOT_P EPTIDE_BONDS_IN_CYCLIC_AMIDES	-1.56	0.033	1.000
GOBP_DEOXYRIBOSE_PHOSPHATE_METABOLIC_PROCESS	-1.56	0.022	1.000
GOBP_INNER_MITOCHONDRIAL_MEMBRANE_ORGANIZATION	-1.56	0.010	1.000
GOBP_NEGATIVE_REGULATION_OF_VIRAL_ENTRY_INTO_HOST_CELL	-1.56	0.020	1.000
GOBP_HISTONE_H4_ACETYLATION	-1.56	0.003	1.000
GOBP_POSITIVE_REGULATION_OF_LEUKOCYTE_CHEMOTAXIS	1.56	0.004	0.303
GOMF_INTRAMOLECULAR_TRANSFERASE_ACTIVITY	-1.56	0.028	1.000
GOBP_AXON_EXTENSION	1.56	0.003	0.304
GOBP_REGULATION_OF_CENTROSOME_CYCLE	-1.56	0.018	1.000
GOBP_CELLULAR_RESPONSE_TO_EXTRACELLULAR_STIMULUS	1.56	0.000	0.304

GOBP_NEGATIVE_REGULATION_OF_DNA_REPLICATION	-1.56	0.015	1.000
GOBP_OLEFINIC_COMPOUND_BIOSYNTHETIC_PROCESS	1.56	0.033	0.303
GOMF_CALCIIUM_ACTIVATED_CATION_CHANNEL_ACTIVITY	1.56	0.033	0.303
GOBP_PYRIMIDINE_NUCLEOSIDE_TRIPHOSPHATE_BIOSYNTHETIC_PROCESS	-1.56	0.021	1.000
GOBP_POSITIVE_REGULATION_OF_EPITHELIAL_CELL_APOPTOTIC_PROCESS	1.55	0.038	0.303
GOCC_PROTEASOME_COMPLEX	-1.55	0.017	1.000
GOBP_NEGATIVE_REGULATION_OF_ENDOPLASMIC_RETICULUM_STRESS_INDUCED_INTRINSIC_APOPTOTIC_SIGNALING_PATHWAY	-1.55	0.033	1.000
GOMF_TRANSLATION_INITIATION_FACTOR_ACTIVITY	-1.55	0.016	1.000
GOCC_DYNEIN_AXONEMAL_PARTICLE	-1.55	0.041	1.000
GOMF_EXODEOXYRIBONUCLEASE_ACTIVITY	-1.55	0.026	1.000
GOMF_ISOPRENOID_BINDING	-1.55	0.024	1.000
GOMF_STEROL_TRANSPORTER_ACTIVITY	1.55	0.027	0.315
GOBP_CEREBELLAR_CORTEX_DEVELOPMENT	-1.55	0.017	1.000
GOBP_NEGATIVE_REGULATION_OF_ORGANELLE_ORGANIZATION	-1.55	0.001	1.000
GOBP_REGULATION_OF_DNA_DAMAGE_CHECKPOINT	-1.55	0.036	1.000
GOBP_LOW_DENSITY_LIPOPROTEIN_PARTICLE_CLEARANCE	1.55	0.037	0.315
GOCC_PROTEASOME_REGULATORY_PARTICLE	-1.55	0.035	1.000
GOBP_POSITIVE_REGULATION_OF_STEM_CELL_PROLIFERATION	-1.55	0.038	1.000
GOBP_DNA_TEMPLATED_TRANSCRIPTION_ELONGATION	-1.55	0.006	1.000
GOBP_MICROTUBULE_ORGANIZING_CENTER_LOCALIZATION	-1.55	0.024	1.000
GOBP_NEURON_DEATH	1.55	0.000	0.317
GOBP_NEGATIVE_REGULATION_OF_MYOTUBE_DIFFERENTIATION	-1.55	0.033	1.000
GOBP_MITOPHAGY	1.54	0.038	0.317
GOBP_PEPTIDYL_ARGININE_METHYLATION	-1.54	0.042	1.000
GOMF_PROTEIN_METHYLTRANSFERASE_ACTIVITY	-1.54	0.006	1.000
GOBP_REGULATION_OF_PROTEIN_LOCALIZATION_TO_NUCLEUS	-1.54	0.004	1.000
GOBP_AXONEME_ASSEMBLY	1.54	0.007	0.327
GOBP_POSITIVE_REGULATION_OF_LEUKOCYTE_MIGRATION	1.54	0.009	0.325
GOMF_PHOSPHATIDIC_ACID_BINDING	-1.54	0.025	1.000
GOBP_MICROTUBULE_DEPOLYMERIZATION	-1.54	0.028	1.000
GOBP_POSITIVE_REGULATION_OF_MITOCHONDRIAL_TRANSLATION	-1.54	0.030	1.000
GOBP_NEGATIVE_REGULATION_OF_MUSCLE_CELL_APOPTOTIC_PROCESS	1.54	0.012	0.327
GOBP_REGULATION_OF_DNA_STRAND_ELONGATION	-1.54	0.047	1.000
GOBP_DOSAGE_COMPENSATION	-1.54	0.034	1.000

GOMF_TRNA_SPECIFIC_RIBONUCLEASE_ACTIVITY	-1.54	0.038	1.000
GOCC_TRANSFERASE_COMPLEX_TRANSFERRING_PHOSPHORUS_CONTAINING_GROUPS	-1.54	0.000	1.000
GOBP_OOCYTE_MATURATION	-1.54	0.038	1.000
GOCC_MICROTUBULE	-1.54	0.000	1.000
GOMF_PROTEIN_CARRIER_CHAPERONE	-1.53	0.033	1.000
GOBP_NEURON_CELLULAR_HOMEOSTASIS	1.53	0.045	0.331
GOMF_CADHERIN_BINDING	-1.53	0.000	1.000
GOBP_NEGATIVE_REGULATION_OF_SYSTEMIC_ARTERIAL_BLOOD_PRESSURE	-1.53	0.039	1.000
GOBP_REGULATION_OF_CELL_MIGRATION_INVOLVED_IN_SPROUTING_ANGIOGENESIS	1.53	0.012	0.335
GOBP_NUCLEOSIDE_TRIPHOSPHATE_BIOSYNTHETIC_PROCESS	-1.53	0.010	1.000
GOBP_COGNITION	1.53	0.000	0.334
GOBP_BONE_MORPHOGENESIS	-1.53	0.011	1.000
GOBP_HISTONE_H3_K9_METHYLATION	-1.53	0.026	1.000
GOBP_HISTONE_DEACETYLATION	-1.53	0.006	1.000
GOBP_CELLULAR_RESPONSE_TO_CORTICOSTEROID_STIMULUS	1.53	0.023	0.335
GOBP_NEGATIVE_REGULATION_OF_INTRINSIC_APOPTOTIC_SIGNALING_PATHWAY_BY_P53_CLASS_MEDIATOR	1.53	0.048	0.334
GOBP_PROTEIN_HETEROOLIGOMERIZATION	-1.53	0.026	1.000
GOBP_REGULATION_OF_CELL_CYCLE_G1_S_PHASE_TRANSITION	-1.53	0.003	1.000
GOBP_ORGANELLE_TRANSPORT_ALONG_MICROTUBULE	1.53	0.013	0.334
GOBP_EMBRYONIC_SKELETAL_JOINT_DEVELOPMENT	-1.53	0.037	1.000
GOBP_MUSCLE_CELL_APOPTOTIC_PROCESS	1.53	0.020	0.333
GOBP_POSITIVE_REGULATION_OF_REACTIVE_OXYGEN_SPECIES_METABOLIC_PROCESS	1.53	0.011	0.331
GOCC_SMALL_RIBOSOMAL_SUBUNIT	-1.53	0.016	1.000
GOBP_NEGATIVE_REGULATION_OF_EPITHELIAL_CELL_DIFFERENTIATION	-1.53	0.021	1.000
GOBP_REGULATION_OF_MEIOTIC_NUCLEAR_DIVISION	-1.53	0.046	1.000
GOMF_BETA_TUBULIN_BINDING	1.53	0.030	0.331
GOCC_PHOTORECEPTOR_CONNECTING_CILIUM	1.53	0.024	0.331
GOBP_ASTROCYTE_ACTIVATION	1.53	0.049	0.329

GOBP_GMP_METABOLIC_PROCESS	-1.53	0.023	1.000
GOBP_REGULATION_OF_TRANSLATIONAL_INITIATION	-1.53	0.013	1.000
GOCC_PROTEIN_ACETYLTRANSFERASE_COMPLEX	-1.53	0.011	1.000
GOBP_CYTOCHROME_COMPLEX_ASSEMBLY	-1.52	0.033	1.000
GOBP_HISTONE_H3_K4_TRIMETHYLATION	-1.52	0.043	1.000
GOBP_REGULATION_OF_ACTIN_FILAMENT_BASED_MOVEMENT	-1.52	0.029	1.000
GOCC_INTEGRIN_COMPLEX	-1.52	0.014	1.000
GOBP_REGULATION_OF_ICOSANOID_SECRETION	1.52	0.050	0.334
GOBP_REGULATION_OF_ATP_DEPENDENT_ACTIVITY	-1.52	0.016	1.000
GOBP_SEMAPHORIN_PLEXIN_SIGNALING_PATHWAY	1.52	0.026	0.332
GOBP_CELLULAR_RESPONSE_TO_ACID_CHEMICAL	1.52	0.007	0.330
GOBP_REGULATION_OF_MITOCHONDRIAL_GENE_EXPRESSION	-1.52	0.035	1.000
GOBP_POSITIVE_REGULATION_OF_NEURON_DEATH	1.52	0.003	0.329
GOMF_CYTOSKELETAL_MOTOR_ACTIVITY	-1.52	0.007	1.000
GOBP_NEGATIVE_REGULATION_OF_NEURON_PROJECTION_DEVELOPMENT	1.52	0.004	0.330
GOCC_MITOCHONDRIAL_SMALL_RIBOSOMAL_SUBUNIT	-1.52	0.032	1.000
GOBP_DNA_DAMAGE_RESPONSE_SIGNAL_TRANSDUCTION_BY_P53_CLASS_MEDIATOR	1.52	0.025	0.329
GOBP_PURINE_NUCLEOSIDE_MONOPHOSPHATE_METABOLIC_PROCESS	-1.52	0.030	1.000
GOMF_INWARD_RECTIFIER_POTASSIUM_CHANNEL_ACTIVITY	1.52	0.043	0.327
GOBP_REGULATION_OF_LEUKOCYTE_MIGRATION	1.52	0.000	0.327
GOBP_RESPONSE_TO_LEUKEMIA_INHIBITORY_FACTOR	-1.52	0.011	1.000
GOBP_PROTEIN_IMPORT_INTO_MITOCHONDRIAL_MATRIX	-1.52	0.047	1.000
GOBP_REGULATION_OF_URINE_VOLUME	-1.52	0.033	1.000
GOBP_C21_STEROID_HORMONE_METABOLIC_PROCESS	1.52	0.037	0.328
GOBP_POSITIVE_REGULATION_OF_PROTEIN_LOCALIZATION_TO_NUCLEUS	-1.52	0.006	1.000
GOBP_AXIS_ELONGATION	-1.52	0.031	1.000
GOMF_TRANSLATION_REGULATOR_ACTIVITY_NUCLEIC_ACID_BINDING	-1.51	0.008	1.000
GOBP_REGULATION_OF_PEPTIDYL_LYSINE_ACETYLTATION	-1.51	0.008	1.000
GOBP_REGULATION_OF_PROTEIN_ACETYLTATION	-1.51	0.015	1.000
GOBP_PROTEIN_LOCALIZATION_TO_VACUOLE	1.51	0.029	0.333
GOBP_NEGATIVE_REGULATION_OF_TELOMERE_MAINTENANCE_VIA_TELOMERE_LENGTHENING	-1.51	0.038	1.000
GOBP_REGULATION_OF_FATTY_ACID_TRANSPORT	1.51	0.046	0.331
GOBP_PURINE_NUCLEOBASE_METABOLIC_PROCESS	-1.51	0.045	1.000

GOBP_LUNG_MORPHOGENESIS	-1.51	0.016	1.000
GOBP_MITOCHONDRIAL_DNA_REPLICATION	-1.51	0.049	1.000
GOBP_POSITIVE_REGULATION_BY_HOST_OF_VIRAL_TRANSCRIPTION	-1.51	0.042	1.000
GOBP_TELOMERE_CAPPING	-1.51	0.033	1.000
GOBP_DNA_MODIFICATION	-1.51	0.011	1.000
GOBP_POSITIVE_REGULATION_OF_CILIUM_ASSEMBLY	-1.51	0.029	1.000
GOBP_RIBOSE_PHOSPHATE_BIOSYNTHETIC_PROCESS	-1.51	0.001	1.000
GOBP_ESTABLISHMENT_OF_CELL_POLARITY	-1.51	0.007	1.000
GOBP_REGULATION_OF_RECEPTOR_RECYCLING	1.51	0.048	0.335
GOMF_OXIDOREDUCTASE_ACTIVITY_ACTING_ON_NAD_P_H_QUINONE_OR_SIMILAR_COMPOUND_AS_ACCEPTOR	1.51	0.016	0.334
GOBP_POSITIVE_REGULATION_OF_HISTONE_H3_K4_METHYLATION	-1.51	0.037	1.000
GOMF_MICROTUBULE_BINDING	-1.51	0.000	1.000
GOMF_XENOBIOTIC_TRANSMEMBRANE_TRANSPORTER_ACTIVITY	1.51	0.042	0.334
GOBP_NEGATIVE_REGULATION_OF_BONE_REMODELING	1.51	0.044	0.333
GOBP_GLYCOSYL_COMPOUND_CATABOLIC_PROCESS	1.51	0.030	0.331
GOBP_POSITIVE_REGULATION_OF_TOR_SIGNALING	1.51	0.026	0.330
GOBP_GLYCEROL_ETHER_METABOLIC_PROCESS	-1.51	0.046	1.000
GOBP_PHOTORECEPTOR_CELL_MAINTENANCE	1.51	0.028	0.330
GOMF_NUCLEAR_LOCALIZATION_SEQUENCE_BINDING	-1.51	0.045	1.000
GOBP_NEGATIVE_REGULATION_OF_CELL_DIVISION	-1.51	0.042	1.000
GOBP_CHRONIC_INFLAMMATORY_RESPONSE	-1.51	0.041	1.000
GOCC_CHROMOCENTER	-1.51	0.038	1.000
GOCC_STEREOCILIUM_TIP	1.51	0.037	0.331
GOBP_NEGATIVE_REGULATION_OF_I_KAPPAB_KINASE_NF_KAPPAB_SIGNALING	1.51	0.036	0.330
GOBP_MOTILE_CILIUM_ASSEMBLY	1.51	0.012	0.329
GOBP_NEGATIVE_REGULATION_OF_SMOOTH_MUSCLE_CELL_PROLIFERATION	1.51	0.028	0.328
GOMF_OXIDOREDUCTASE_ACTIVITY_ACTING_ON_A_SULFUR_GROUP_OF_DONORS	1.50	0.006	0.327
GOBP_ANTEROGRADE_AXONAL_TRANSPORT	1.50	0.017	0.325
GOBP_REGULATION_OF_TELOMERASE_ACTIVITY	-1.50	0.024	1.000
GOBP_RESPONSE_TO_NERVE_GROWTH_FACTOR	-1.50	0.022	1.000
GOBP_STEROL_METABOLIC_PROCESS	1.50	0.004	0.325

GOBP_NEGATIVE_REGULATION_OF_FATTY_ACID_BIOSYNTHETIC_PROCESS	1.50	0.045	0.327
GOMF_NUCLEOCYTOPLASMIC_CARRIER_ACTIVITY	-1.50	0.046	1.000
GOBP_NEGATIVE_REGULATION_OF_TELOMERE_MAINTENANCE_VIA_TELOMERASE	-1.50	0.039	1.000
GOBP_PROTEIN_LOCALIZATION_TO_LYSOSOME	1.50	0.025	0.328
GOBP_CELLULAR_PIGMENTATION	1.50	0.033	0.327
GOBP_MRNA_CATABOLIC_PROCESS	-1.50	0.001	1.000
GOMF_OXIDOREDUCTASE_ACTIVITY_ACTING_ON_PAIRING_OF_DONORS_WITH_IN_CORPORATION_OR_REDUCTION_OF_MOLECULAR_OXYGEN_REDUCED_FLAVIN_OR_FLAVOPROTEIN_AS_ONE_DONOR_AND_INCORPORATION_OF_ONE_ATOM_OF_OXYGEN	1.50	0.023	0.326

Supplementary Table 4. Sequence of primers used for qPCR.

Gene	Forward primer (5'-3')	Reverse primer (5'-3')
HO-1	ATTCAGAAGGGCCAGGTGA	GGAAGTAGACAGGGGCGAAGA
NOQ1	CCCCGGACTGCACCAGAGC	CTGCAGCAGCCTCCTTCATGGC
OSGIN1	GCAGCAGATGATGCGTGAC	GGAGCCGATGAGGACGAG
18s	CAGAAGGATGTAAAGGATGG	TATTTCTTCTTGGACACACC